

EARTH SCIENCES

**High-Precision Geochronological Constraints on the Duration
of ‘Dinosaurs Pompeii’ and the Yixian Formation**

Yuting Zhong^{1,2}, Magdalena H. Huyskens³, Qing-Zhu Yin^{3,*}, Yaqiong Wang⁴, Qiang Ma^{1,5}, Yi-Gang Xu^{1,2,*}

¹State Key Laboratory of Isotope Geochemistry, Guangzhou Institute of Geochemistry, Chinese Academy of Sciences, Guangzhou 510640, China

²CAS Center for Excellence in Deep Earth Science, Guangzhou 510640, China

³Department of Earth and Planetary Sciences, University of California at Davis, Davis, California 95616-8605, USA

⁴State Key Laboratory of Palaeobiology and Stratigraphy, Nanjing Institute of Geology and Palaeontology and Center for Excellence in Life and Paleoenvironment, Chinese Academy of Sciences, Nanjing 210008, China

⁵State Key Laboratory of Geological Processes and Mineral Resources, School of Earth Sciences, China University of Geosciences, Wuhan 430074, China

***Corresponding authors.**

Emails: yigangxu@gig.ac.cn; qyin@ucdavis.edu

The Early Cretaceous Jehol Biota, renowned for its exceptionally well preserved volcanic-influenced ecosystem, was buried in lacustrine and occasionally fluvial sediments, notably the Huajiying, Yixian, and Jiufotang Formations in northern Hebei

and western Liaoning or equivalent ash-interbedding sediments in neighboring areas [1–3] (Fig. 1). It includes large amount of evolutionarily significant taxonomy, e.g. feathered dinosaurs, early birds, mammals and flowering plants, representing one of the most diversified terrestrial biotas of the Mesozoic [1,2,4].

The evolutionary radiation of the Jehol Biota can be broadly divided to three phases [5], with the first phase limited to a small area in northern Hebei (Huajiying Formation), the second phase expanding to western Liaoning (Yixian Formation) marking the greatest diversification, and the third phase (Jiufotang Formation) representing the widest distribution. Accordingly, it is crucial to precisely determine the timing and duration of the Yixian Formation. Despite considerable efforts in the past two decades attempting to achieve this goal, the published results (Fig. 1D) are confusing and inadequate: (a) Despite its lowermost stratigraphic locations [3], the existing ages of the Lujiatun Unit (LJT Unit for short) are younger than those of the immediate overlying Lower Lava Unit. The ages of the upper Yixian Formation are younger than the overlying Jiufotang Formation. It therefore casts serious doubt on the robustness of these dating results. (b) Although most of the published ages of the Yixian Formation with the exception of those for LJT Unit define an overall younging direction following the stratigraphic column from bottom to top, the ages within individual units do not always show a consistency in stratigraphically upward decreasing trend. These problems may stem either from inaccurate stratigraphic information of some dated samples, or from inconsistency of inter-laboratory analyses, between different dating methods (i.e., $^{40}\text{Ar}/^{39}\text{Ar}$ and U-Pb dating by either laser ablation or secondary ion probe), and relatively large analytical uncertainties, which are inadequate for the purpose of establishing a chronostratigraphic

framework. We therefore use U-Pb chemical abrasion-isotope dilution-isotope ratio mass spectrometry (CA-ID-IRMS) dating technique with a typical analytical precision <0.05% to date single zircons from volcanic tuff layers collected from the top (CY18-20), middle (CY17-17) and bottom (CY17-18 and CY17-9) of the Yixian Formation in the Jin-Yang basin (Fig. 1C), in order to tightly constrain its absolute age and duration.

The new CA-ID-IRMS ages show significant improvement in analytical precision compared with literature data (Figs. 1D, E). Our new ages collectively provide very tight constraints on the onset at 125.755 ± 0.061 Ma (CY17-9) and termination at 124.122 ± 0.048 Ma (CY18-20) of the Yixian Formation, respectively, bracketing its duration to 1.633 ± 0.078 Myr. It is significantly shorter than the previous broad range estimates of ~2 - 7 Myr [6]. The fossil preservation in the LJT Unit is often referred to as “Chinese Pompeii” for dinosaurs and other fossils due to rapidly deposited catastrophic pyroclastic flows [7]. Our new age constraints with the extraordinarily short duration of LJT Unit $<71 \pm 86$ Kyr, support this sudden nature of the deposition event(s) that preserving fossils in three-dimensional structures with gestures.

Some argued that the JSG and LJT units are stratigraphically equivalent primarily based on prior chronological data [8]. However, the two units show considerably different petrographic facies, mineralogical characteristics and geochemical compositions (Supplementary Texts 1, 2), suggesting that the two units represent separate depositional events. The difference in the two units is further confirmed by the younger age of CY17-17 from JSG Unit than that of the LJT Unit. The ages of the LJT and JSG units are resolvable given the extraordinary precision achieved in this study, with JSG Unit being

sequentially deposited later than LJT Unit, in agreement with their stratigraphic relationship observed in the field and cores [3].

The refined duration of the Yixian Formation also yields important insights on the duration of the JSG lacustrine deposits. The sedimentary cyclicity was interpreted as periodic lake-level fluctuations plausibly caused by climatic changes that in turn may be orbitally forced Milankovitch cycles [3,9]. If so, our study effectively rules out that the lacustrine cyclostratigraphy documented in part of the Yixian Formation was driven by orbital eccentricity, but more likely obliquity or precession signals. Our new data indicate that the entire Yixian Formation is only 1.633 ± 0.078 Myr max, which means that the JSG Unit within Yixian Formation should be <1.633 Myr. This would clearly exclude the possibility to interpret the 2 m cycle as 100 Kyr eccentricity cycle for a 41 m JSG Unit. It is possible that the sedimentation rates of lacustrine environments between the studied outcrops and drill cores are highly variable, obtaining accurate Milankovitch cycle signals from the terrestrial sediments remain a challenging goal without further high-resolution geochronological constraints.

SUPPLEMENTARY DATA

Supplementary data are available at *NSR* online.

FUNDING

This work was supported by the National Natural Science Foundation of China (41688103 and 41873018) and the Strategic Priority Research Program (B) of the Chinese Academy of Sciences (XDB18000000).

REFERENCES

1. Zhou ZH. *Natl Sci Rev* 2014; **1**: 543–559.
2. Pan YH, Sha JG, and Zhou ZH *et al.* *Cretac Res* 2013; **44**: 30–38.
3. Wang YQ, Olsen PE, and Sha JG *et al.* *Palaeogeogr Palaeoclimatol Palaeoecol* 2016; **464**: 110–133.
4. Zhou ZH, Barrett PM, and Hilton J. *Nature* 2003; **421**: 807–814.
5. Zhou ZH, Wang Y, and Xu X *et al.* The Jehol Biota: an exceptional window into Early Cretaceous terrestrial ecosystems. In: Nicholas F (ed.). *Terrestrial Conservation Lagerstätten: Windows into the Evolution of Life on Land*. Dunedin Academic Press, 2017, 169–214.
6. Chang SC, Zhang HC, and Renne PR *et al.* *Palaeogeogr Palaeoclimatol Palaeoecol* 2009; **280**: 94–104.
7. Jiang BY, Harlow GE, and Wohletz K *et al.* *Nat Commun* 2014; **5**: 1–7.
8. Chang SC, Gao KQ, and Zhou CF *et al.* *Palaeogeogr Palaeoclimatol Palaeoecol* 2017; **487**: 399–406.
9. Wu HC, Zhang SH, and Jiang GQ *et al.* *Palaeogeogr Palaeoclimatol Palaeoecol* 2013; **385**: 221–228.
10. Renne PR, Mundil R, and Balco G *et al.* *Geochim Cosmochim Acta* 2010; **74**: 5349–5367.

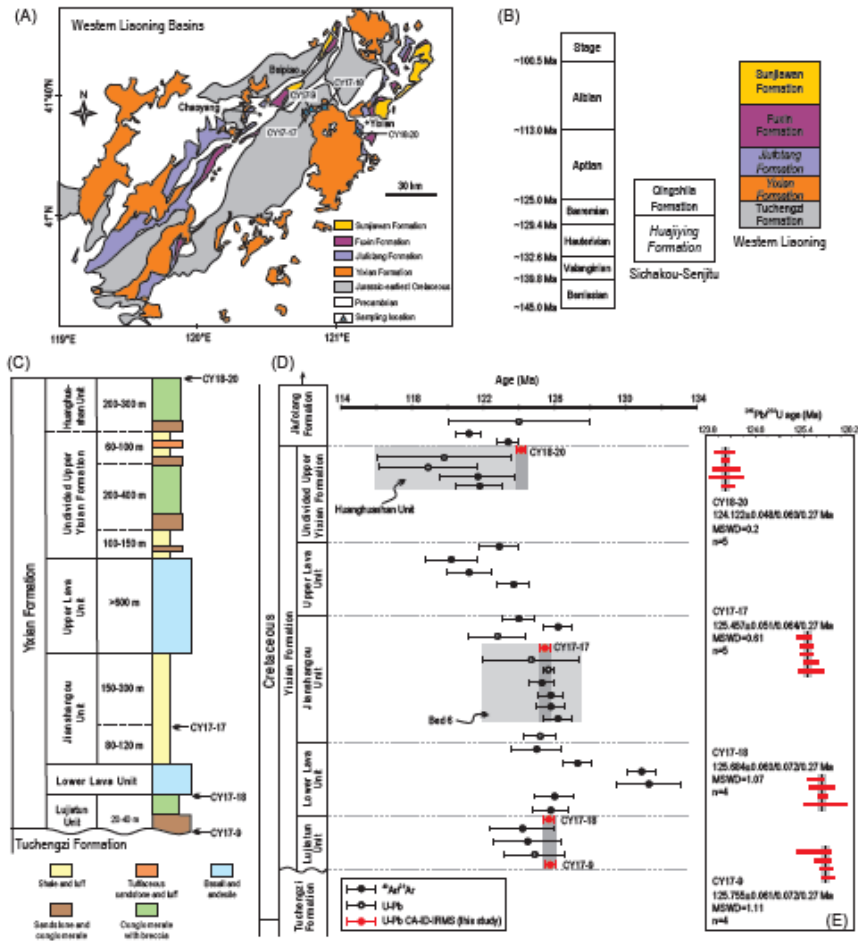


Figure 1. (A) The schematic geological map of western Liaoning Province (modified from Wang et al. [3]) with the sampling locations. (B) Early Cretaceous stratigraphic columns in northern Hebei and western Liaoning. Three formations, in *italics*, namely Huajiying, Yixian and Jiufotang Formations are the main hosts of Jehol Biota. (C) Composite stratigraphic column (modified after Zhou et al. [4]) and the sampling horizons of the Yixian Formation. (D) A summary plot comparing literature age data (Supplementary Table S1) with our new U-Pb CA-ID-IRMS results for the Yixian Formation. The $^{40}\text{Ar}/^{39}\text{Ar}$ dates are corrected using the decay constant of Renne et al. [10] and all reported uncertainties are in 2σ . Red circles denote U-Pb ages obtained in this study, with the full systematic uncertainties (uncertainty Z) for comparison with $^{40}\text{Ar}/^{39}\text{Ar}$ dates. (E) Ranked-age plots for single zircon U-Pb analyses for CY18-20, CY17-17, CY17-18, and CY17-9.

**High Precision Geochronological Constraints on the Duration of ‘Dinosaur Pompeii’
and the Yixian Formation**

Supporting Figures S1-S15

Supplementary Texts 1-3

Supplementary Tables S1-S4

Supporting Figures

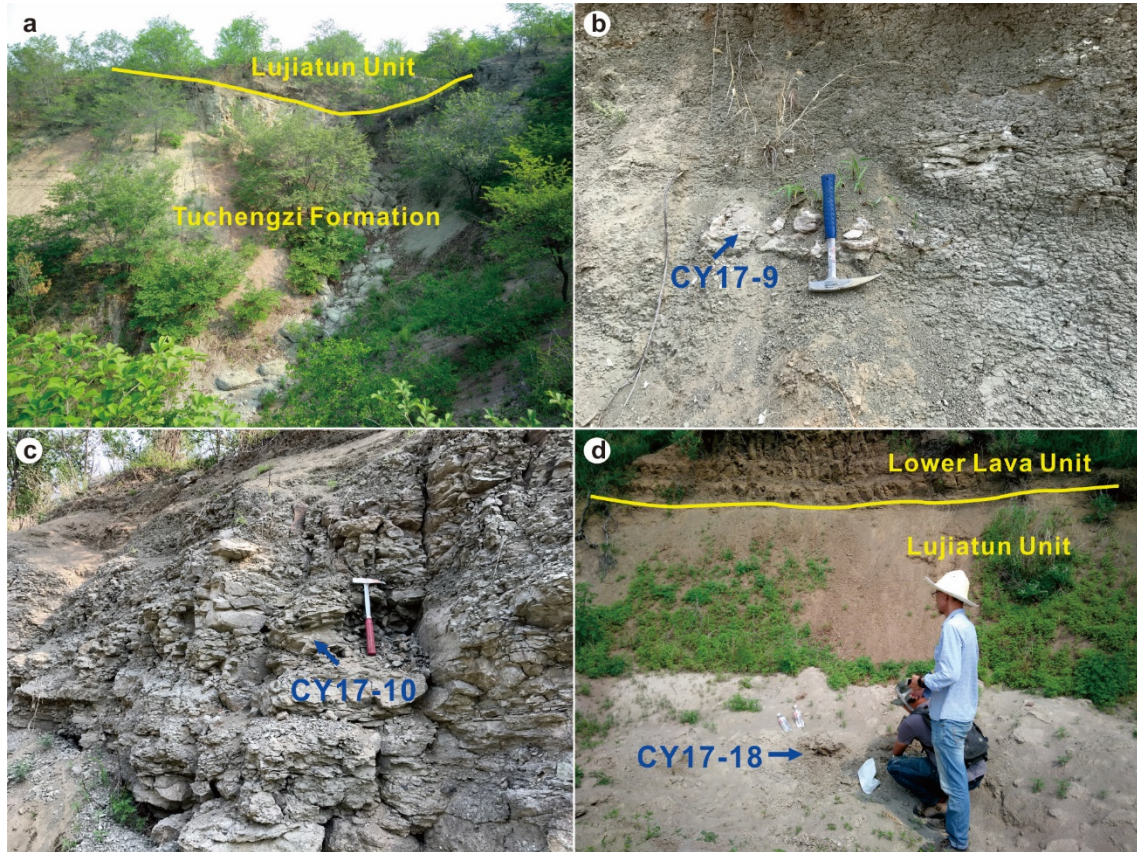


Fig. S1. Field photographs showing the sampling locations from LJT Unit. (a) The contact between Tuchengzi Formation and LJT Unit of Yixian Formation ($41^{\circ}36'1.6''\text{N}$, $120^{\circ}48'57.1''\text{E}$). (b) Field appearance of sample CY17-9, at the bottom of LJT Unit. (c) Field appearance of sample CY17-10, at the lower part of LJT Unit. (d) The contact between LJT and LL units (Yixian Formation), and the field appearance of sample CY17-18.

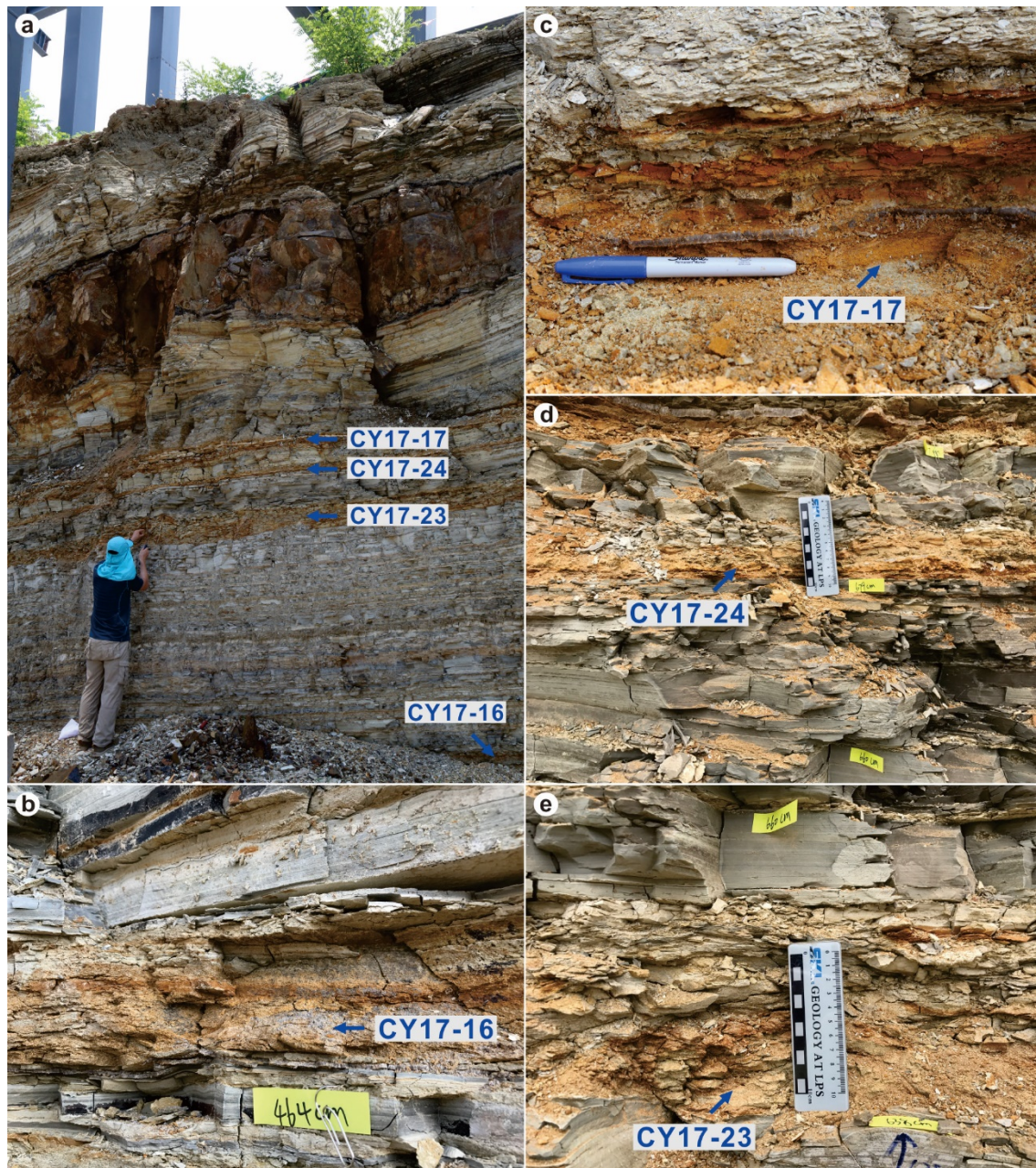


Fig. S2. Field photographs showing the horizons of sample collection at JSG Unit. (a) Overview image of the JSG Unit at the Sihetun Museum. Close-up view of the samples (b) CY17-16, (c) CY17-17, (d) CY17-24, and (e) CY17-23. The yellow sticky note for scale is 1.5 cm in height. The marker in (c) for scale is 14 cm long.



Fig. S3. Field photograph showing sample CY18-20 collected from Huanghuashan Unit.

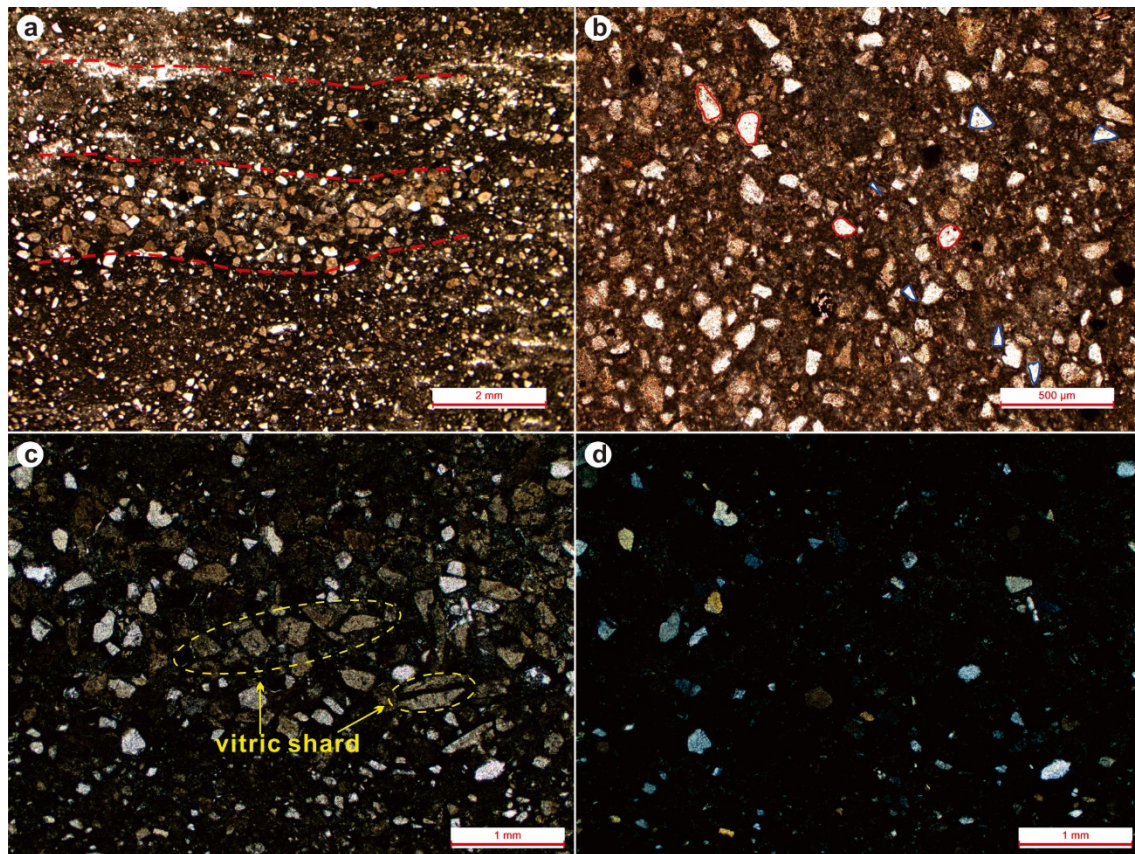


Fig. S4. Photomicrographs of sample CY17-9. (a) The overview shows the micro-bedding texture. (b) The magnified view of the lower part of (a), showing two shapes of quartz are mixed: (1) the volcanic quartz fragments (outlined in blue) are angular, most of them are smaller than 100 μm ; (2) the sedimentary quartz fragments (red circle) are well rounded ($\sim 100 \mu\text{m}$), which represent the addition of terrigenous detrital fractions during the deposition. (c) The close-up view shows vitric shard (0.2-0.6mm long), goes complete extinction under the cross-polarized light (d). (a), (b), and (c) are taken under plane-polarized light, (d) is taken under cross-polarized light.

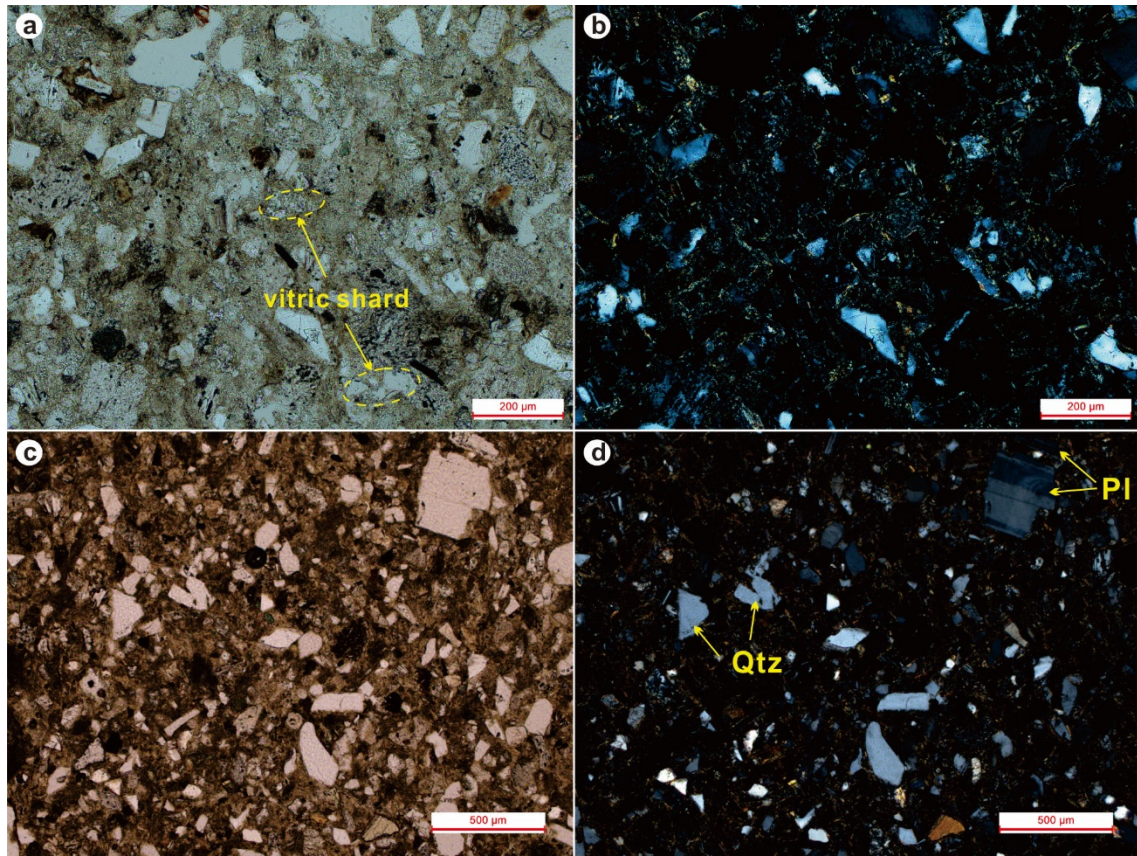


Fig. S5. Photomicrographs of sample CY17-10. (a) and (c) are taken under plane-polarized light, (b) and (d) are taken under cross-polarized light. Pl: plagioclase; Qtz: quartz.

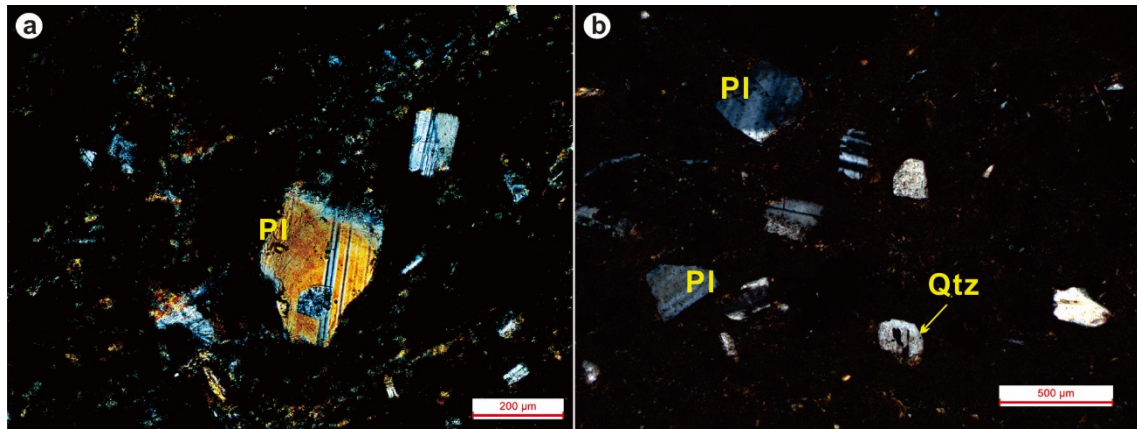


Fig. S6. Photomicrographs of sample CY17-18. All the images are taken under cross-polarized light. Pl: plagioclase; Qtz: quartz.

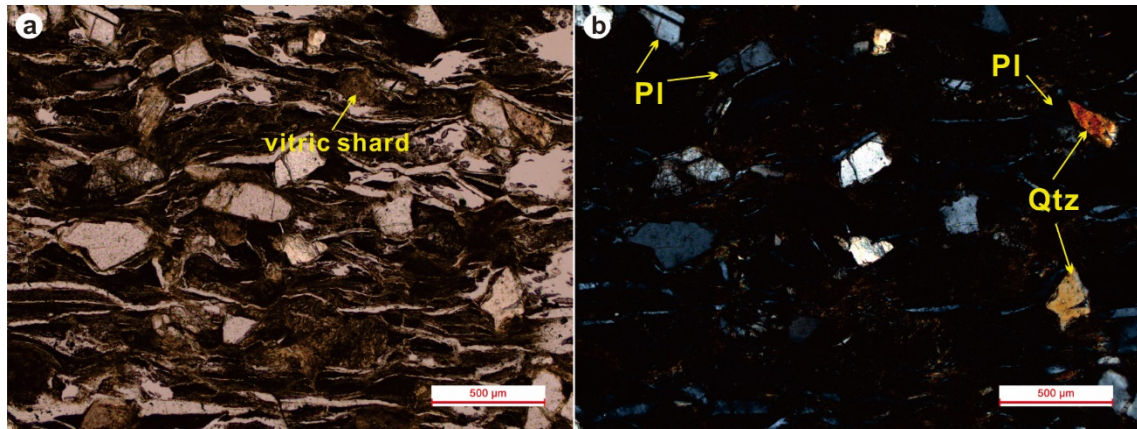


Fig. S7. Photomicrographs of sample CY17-16. (a) is taken under plane-polarized light, and (b) is taken under cross-polarized light. Pl: plagioclase; Qtz: quartz.

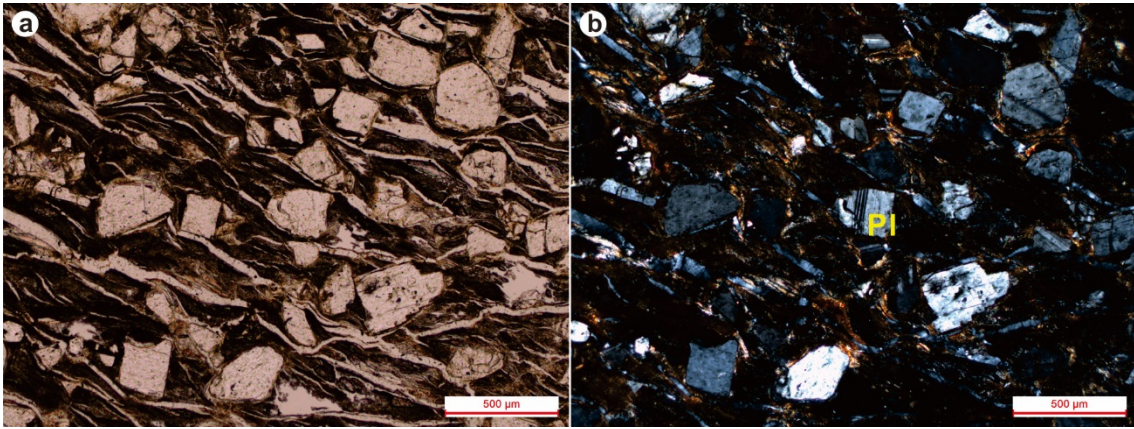


Fig. S8. Photomicrographs of sample CY17-17. (a) is taken under plane-polarized light, and (b) is taken under cross-polarized light. Pl: plagioclase.

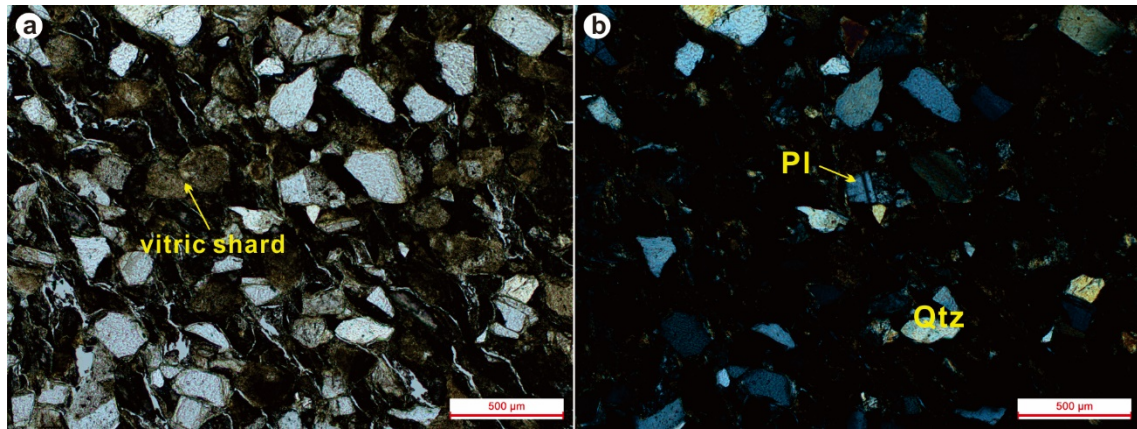


Fig. S9. Photomicrographs of sample CY17-23. (a) is taken under plane-polarized light, and (b) is taken under cross-polarized light. Pl: plagioclase; Qtz: quartz.

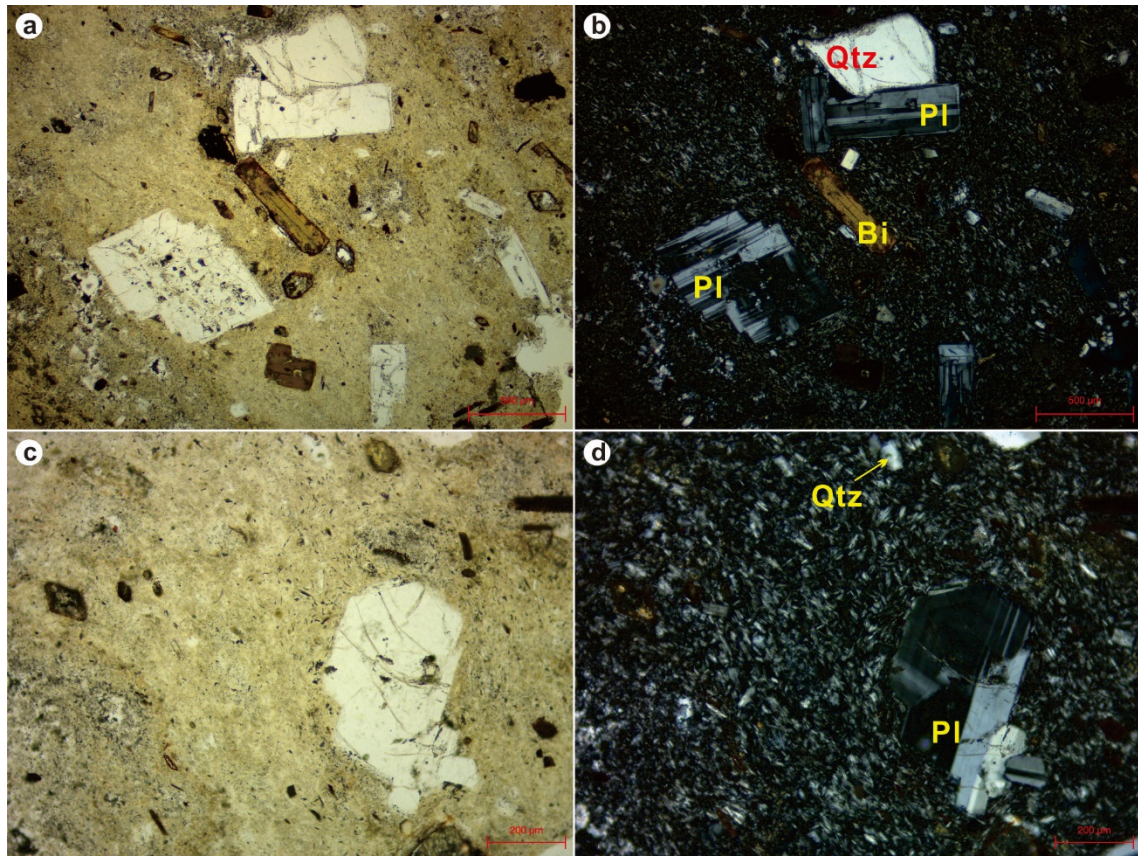


Fig. S10. Photomicrographs of sample CY18-20. (a) and (c) are taken under plane-polarized light, (b) and (d) are taken under cross-polarized light. Pl: plagioclase; Qtz: quartz; Bi: biotite.

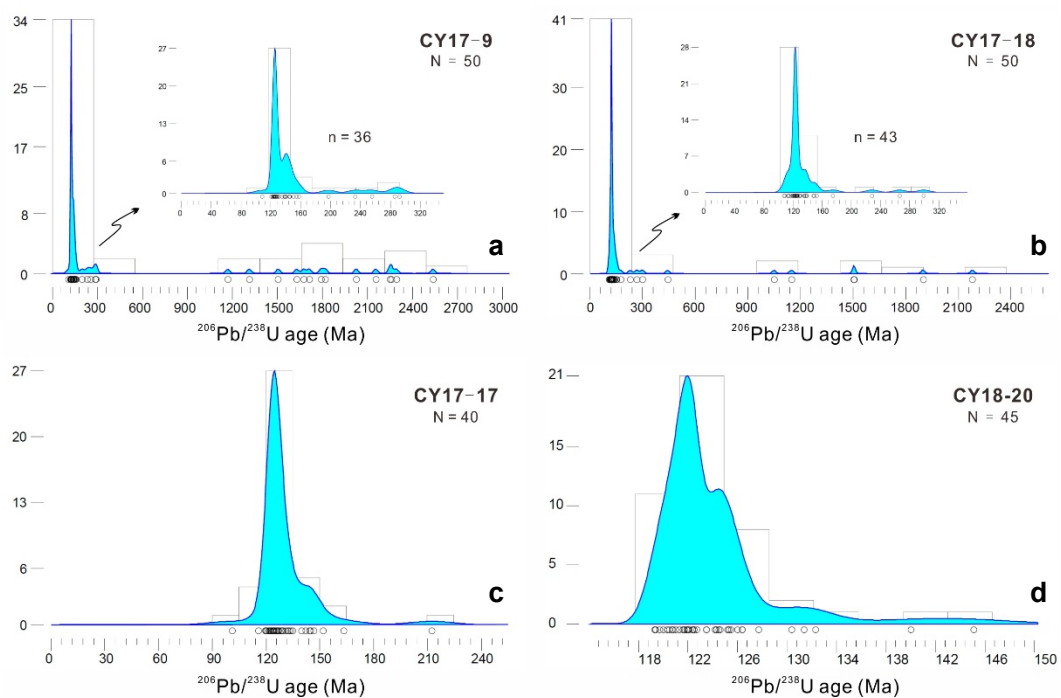


Fig. S11. Kernel density estimation (*I*) of zircons analyzed by laser ablation ICP-MS for samples (a) CY17-9, (b) CY17-18, (c) CY17-17, and (d) CY18-20. All the analyzed zircons are included, regardless of concordance. These results were used as a guide to select the youngest population for higher precision U-Pb dating by CA-ID-IRMS method.



Fig. S12. Images of single zircon grains after leaching procedure (chemical abrasion) for each sample (CY17-9, CY17-18, CY17-17, and CY18-20) that were analyzed by CA-ID-IRMS.

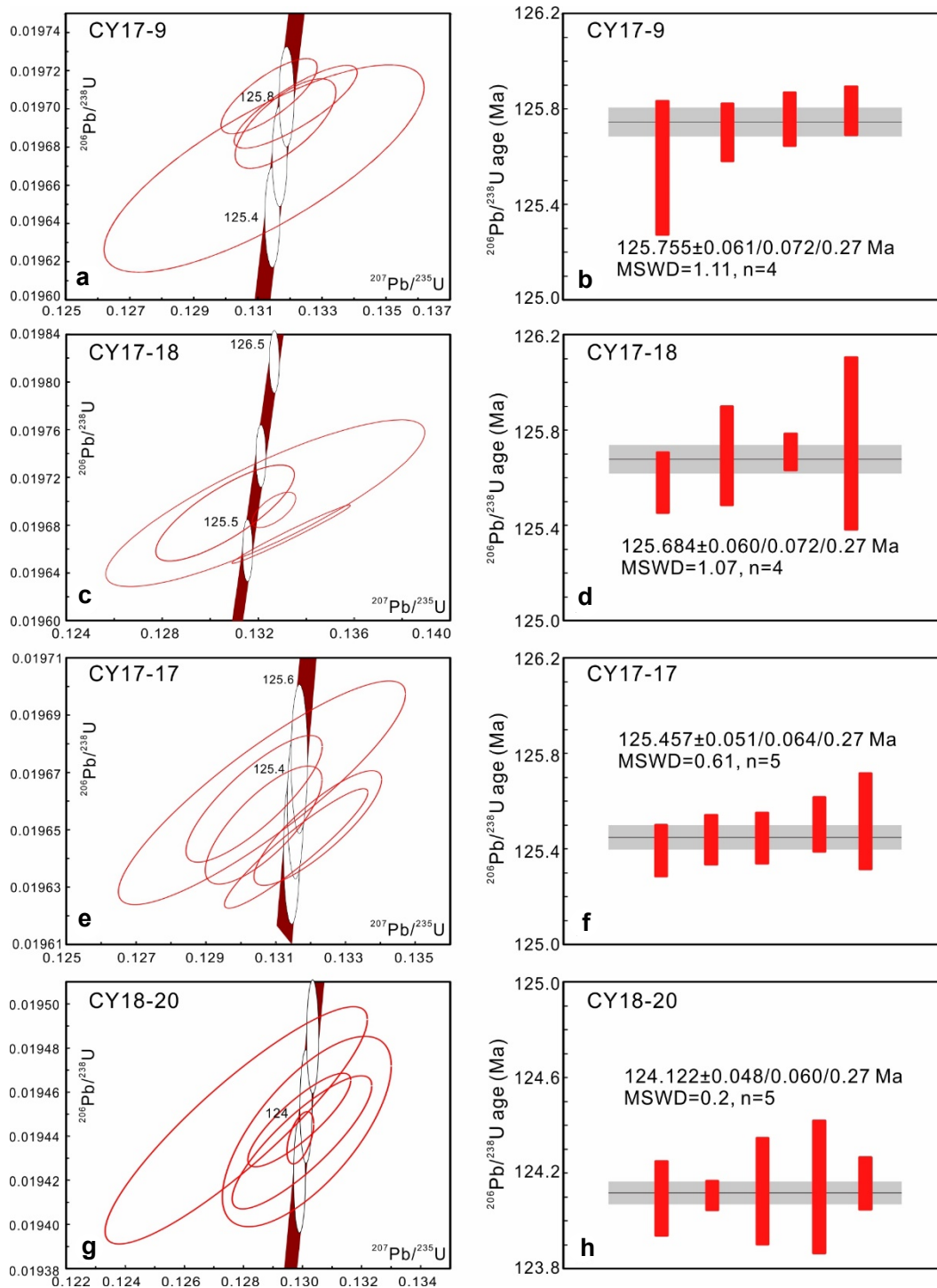


Fig. S13. Concordia diagrams (a, c, e, g) and ranked-age plots (b, d, f, h) show the results from analyzed samples by CA-ID-IRMS. The red color band in the Concordia plots represents the decay constant uncertainty. In the ranked-age plots, each bar represents the date and analytical uncertainty of an individual zircon grain and the grey bar showing the weighted average (95% uncertainty) of all analyzed zircon grains for each sample.

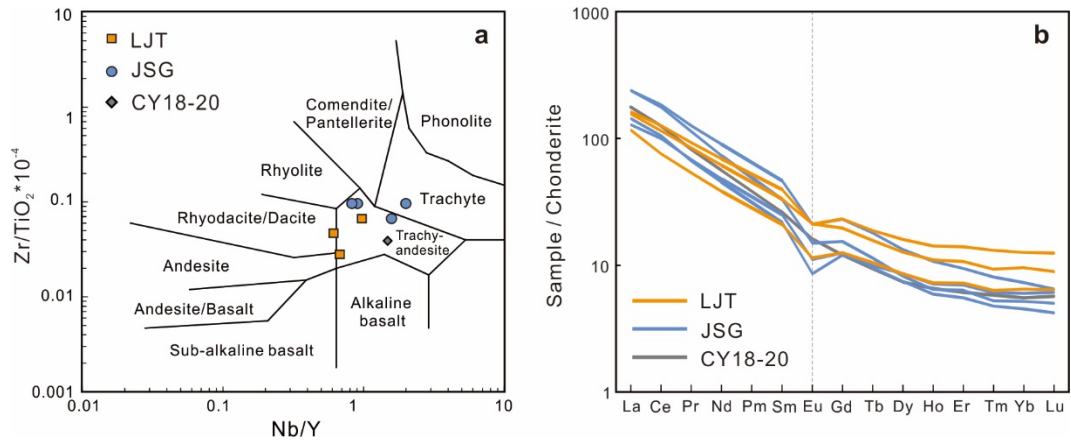


Fig. S14. (a) Nb/Y-Zr/TiO₂ classification diagram (2). (b) Diagram of chondrite-normalized rare earth element (REE) patterns. Normalization values are after Sun and McDonough, (3).

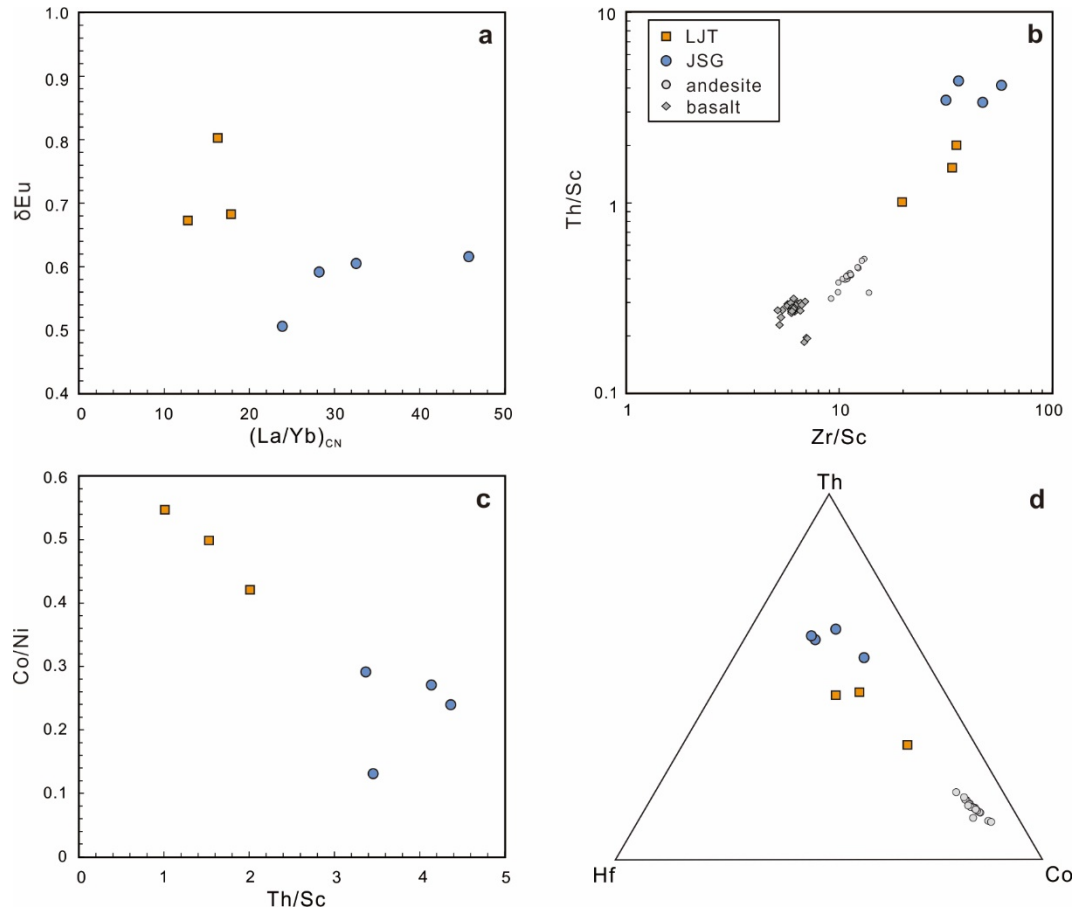


Fig. S15. Plots of (a) $(\text{La}/\text{Yb})_{\text{CN}}-\delta\text{Eu}$, (b) $\text{Zr}/\text{Sc}-\text{Th}/\text{Sc}$ (4), (c) $\text{Th}/\text{Sc}-\text{Co}/\text{Ni}$, and (d) $\text{Th}-\text{Hf}-\text{Co}$ ternary diagrams (5). Also shown in (b) and (d) are the andesites and basalts from Sihetun area, which are compiled from Wang, et al. (6), Gao, et al. (7), Yang and Li, (8).

References

1. P. Vermeesch, On the visualisation of detrital age distributions. *Chem. Geol.* 312, 190–194 (2012).
2. J. A. Winchester, P. A. Floyd, Geochemical discrimination of different magma series and their differentiation products using immobile elements. *Chem. Geol.* 20, 325–343 (1977).
3. S. S. Sun, W. F. McDonough, Chemical and Isotopic Systematics of Oceanic Basalts: Implications for Mantle Composition and Processes. *Geol. Soc. Spec. Pub.* 42, 313–345 (1989).
4. S. R. Taylor, S. M. McLennan, The continental crust: its composition and evolution. Black Scientific Publications, pp. 1–312 (1985).
5. S. M. McLennan, S. Hemming, D. K. McDaniel, G. N. Hanson, Geochemical approaches to sedimentation, provenance, and tectonics, in Johnson, M.J., and Basu, A., eds., *Processes Controlling the Composition of Clastic Sediments*. *Geol. Soc. Spec. Paper* 284, 21–40 (1993).
6. X. R. Wang, S. Gao, X. M. Liu, H. L. Yuan, Z. C. Hu, H. Zhang, X. C. Wang, Geochemistry of high-Mg andesites from the early Cretaceous Yixian Formation, western Liaoning: Implications for lower crustal delamination and Sr/Y variations. *Sci. China D* 49, 904–914 (2006).
7. S. Gao, R. L. Rudnick, W. L. Xu, H. L. Yuan, Y. S. Liu, R. J. Walker, I. S. Puchtel, X. M. Liu, H. Huang, X. R. Wang, J. Yang, Recycling deep cratonic lithosphere and generation of intraplate magmatism in the North China Craton. *Earth Planet. Sc. Lett.* 270, 41–53 (2008).
8. W. Yang, S. G. Li, Geochronology and geochemistry of the Mesozoic volcanic rocks in Western Liaoning: Implications for lithospheric thinning of the North China Craton. *Lithos* 102, 88–117 (2008).

Supplementary Text 1

Samples

Yixian Formation

Underlain by the Tuchengzi Formation and overlain by the Jiufotang Formation, the Yixian Formation is mainly composed of andesites, andesite-breccia, agglomerates, basalts, and the fossil-bearing sedimentary intercalations rich in tuffaceous materials (1). It comprises five units, in an ascending order, Lujiatun (LJT for short), Lower Lava, Jianshangou (JSG for short), Upper Lava units, and undivided Upper Yixian Formation. Among them, LJT and JSG units are the principle hosts of the fossils of the Jehol Biota. The LJT Unit, situated at the base of the Yixian Formation (2), consists of massive tuffaceous sandstone or siltstone (3). Numerous three-dimensionally preserved vertebrate fossils have been recovered, including some specimens preserving behavioral information but with no traces of soft tissues (4,5). For example, the *Mei long* holotype is preserved in a remarkable life tuck-in sleeping (or resting) posture (5). Pyroclastic flows are hypothesized as a potential cause for the mass mortality events and the remarkable preservation (3). In contrast, the JSG Unit is mainly composed of fine laminated sediments and yields abundant flattened vertebrates usually with various soft tissues preserved, e.g., skins, hairs, feathers (1,6,7). For instance, the *Sinosauropteryx prima* has interesting integumentary structures that could provide information about the origin of feathers (1).

Field observations and sampling horizons

Lujiatun Unit. The Lujiatun (LJT for short) Unit is the lowermost unit of the Yixian Formation overlain by the Lower Lava (LL for short) Unit (Figs. S1a and 1d), which is mainly composed of volcanic conglomerates, massive tuffaceous sandstone or siltstone. LJT Unit generally shows little to no stratification (8,9). Three samples have been collected from the LJT Unit. CY17-9 was collected from the bottom of LJT Unit (41°35'59.8"N, 120°48'59.8"E) (Fig. S1b). CY17-10 was collected along the same section as CY17-9, representing the lower part of LJT Unit (41°35'57"N, 120°49'3.1"E). Both of them are grayish white in color (Figs. S1b-c), dense and hard. CY17-18 was collected from the topmost of the LJT Unit (41°36'7.6"N, 120°54'47.5"E), which is about 1.8 meters

below the contact between LJT and LL units (Fig. S1d). CY17-18 is off-white in-color and poorly consolidated.

Jianshangou Unit. Samples were collected from Jianshangou (JSG for short) Unit at the Sihetun section (41°35'18.93"N, 120°47'32.66"E). As show in Fig. S2a, at least 15 layers ($h > 1$ cm) of yellowish tuff were identified within the 4.6-meters thickness section, and all of the tuffs are poorly consolidated. Four tuff samples were collected, CY17-16, CY17-23, CY17-24, and CY17-17 in ascending order and the sampled horizons shown in Fig. S2a. The thicknesses for the sampled tuff layers are 7cm, 14cm, 7cm, and 7cm, respectively. Fossils in the JSG Unit were mainly found below CY17-17 which was dated in this study.

Huanghuashan Unit. The stratigraphy of the Upper Yixian Formation remains controversial. Several units, namely Huanghuashan Unit, Jingangshan Unit, Dawangzhangzi Unit, have been proposed, but the temporal relationship between these units is not assessed yet. Instead of going into specific debates, the Upper Yixian Formation is simply treated as undivided in this study. Nevertheless, the Huanghuashan Unit is considered as on the top of the uppermost fossiliferous unit of the Yixian Formation (10-12), because it is in conformable contact with the overlying Jiufotang Formation. It thus represents the dating target for the termination of the Yixian Formation. Sample CY18-20 was collected at Songbahu section (Fig. S3; 41°28'10.97"N, 121°10'9.72"E).

Petrography of the samples

Lujiatun Unit. The CY17-9 is a poorly to moderately sorted vitric-crystal tuff with angular to sub-rounded grains of quartz and plagioclase feldspar (Fig. S4). There are abundant sickle-shaped vitric fragments, and most of them have been devitrified (Figs. S4c-d). Considering the mixtures of sedimentary quartz and volcanic quartz (Fig. S4b), it is reasonable to classify it as a sedimentary tuff.

Similar to CY17-9, the CY17-10 is a poorly sorted vitric-crystal tuff (Fig. S5). The crystal fragments are dominated by angular to subangular quartz ($>20 - 100 \mu\text{m}$), plagioclase feldspar ($>50 - 200 \mu\text{m}$), and small amounts of biotite. The quartz fragments are often with magmatic corrosion gulfs. Some chicken bone-shaped vitric fragments are observed.

The CY17-18 is a poorly consolidated tuff with small amount of crystal fragments (Fig. S6). Plagioclase ($\sim 100 - 350 \mu\text{m}$) is white-colored with perfect cleavage and albite twin. The quartz fragments ($<100 \mu\text{m}$) are often with magmatic corrosion gulfs. Clasts float in a clayey groundmass of devitrified volcanic glass and very fine ashes.

Jianshangou Unit. All samples collected from JSG Unit are poorly consolidated tuff. During the preparation of thin-section, the textural integrity of the samples were compromised. The descriptions here are therefore only referring to the components.

The CY17-16 is a crystal tuff with plate-like plagioclase (>100 – 250 μm) and small amounts of angular quartz (up to 200 μm) (Fig. S7). Some orange colored vitric shard are observed.

The CY17-17 is a crystal tuff with abundant angular to subangular plagioclase and quartz (both are 100 – 200 μm) (Fig. S8).

The CY17-23 is a poorly consolidated crystal tuff. The crystal fragments include angular to subangular quartz and plagioclase feldspar (both are 100 – 200 μm) (Fig. S9). Some vitric shard and altered plagioclase are observed. In summary, samples CY17-23 and CY17-17 are crystal tuffs and sharing similar compositions.

Huanghuashan Unit. The sample CY18-20 is greyish in color and has a porphyritic texture (Fig. S10). The predominant phenocrysts are plagioclase (~10 vol%), biotite (~5 vol%), and quartz (~3 vol%). Plagioclase and biotite (both ~500 μm) occur as euhedral grains. The groundmass consists of fine-grained quartz and lath-shaped plagioclase (Fig. S10). Minor opaque minerals and zircon grains occur in the groundmass. Geochemical analyses suggest it is a trachyandesite (see Section ‘Major and trace elemental compositions’ below).

References

1. P. J. Chen, Z. M. Dong, S. N. Zhen, An exceptionally well-preserved theropod dinosaur from the Yixian Formation of China. *Nature* 391, 147–152 (1998).
2. Y. Q. Wang, P. E. Olsen, J. G. Sha, X. G. Yao, H. Y. Liao, Y. H. Pan, S. Kinney, X. L. Zhang, X. Rao, Stratigraphy, correlation, depositional environments, and cyclicity of the Early Cretaceous Yixian and ?Jurassic-Cretaceous Tuchengzi formations in the Sihetun area (NE China) based on three continuous cores. *Palaeogeogr Palaeoclimatol Palaeoecol* 464, 110–133 (2016).
3. B.Y. Jiang, G. E. Harlow, K. Wohletz, Z. H. Zhou, J. Meng, New evidence suggests pyroclastic flows are responsible for the remarkable preservation of the Jehol biota. *Nat Commun* 5, 1–7 (2014).
4. X. Xu, Y. N. Cheng, X. L. Wang, An unusual oviraptorosaurian dinosaur from China. *Nature* 417, 291–293 (2002).
5. X. Xu, M. A. Norell, A new troodontid dinosaur from China with avian-like sleeping posture. *Nature* 431, 838–841 (2004).
6. Z. H. Zhou, The origin and early evolution of birds: discoveries, disputes, and perspectives from fossil evidence. *Naturwissenschaften* 91, 455–471 (2004).
7. F. C. Zhang, S. L. Kearns, P. J. Orr, M. J. Benton, Z. H. Zhou, D. Johnson, X. Xu, X. L. Wang, Fossilized melanosomes and the colour of Cretaceous dinosaurs and birds. *Nature* 463, 1075–1078 (2010).
8. Z. H. Zhou, P. M. Barrett, J. Hilton, An exceptionally preserved Lower Cretaceous ecosystem. *Nature* 421, 807–814 (2003).
9. B. Y. Jiang, J. G. Sha, Preliminary analysis of the depositional environments of the Lower Cretaceous Yixian Formation in the Sihetun area, western Liaoning, China. *Cretac. Res.* 28, 183–193 (2007).
10. W. L. Wang, L. J. Zhang, S. L. Zheng, Y. Zheng, H. Zhang, Z. T. Li, F. L. Yang, A new study on the stratotype and biostratigraphy of the Yixian Stage in the Yixian-Beipiao region, Liaoning-Establishment and study of the stratotype of the Yixian Stage (in Chinese with English abstract). *Acta Geol. Sin.* 78, 433–447 (2004).
11. H. Zhang, F. L. Yang, L. J. Zhang, Z. T. Li, W. L. Wang, B. Ma, W. G. Sun, S. L. Zheng, Y. J. Zheng, New progress in the study of Huanghuashan Breccia in Yixian county, western Liaoning (in Chinese with English abstract). *Acta Geol. Sin.* 25, 321–326 (2004).
12. H. Zhang, X. M. Liu, W. Chen, Z. T. Li, F. L. Yang, The age of the top of the Yixian Formation in the Beipiao-Yixian area, western Liaoning, and its importance (in Chinese with English abstract). *Geol. China* 32, 596–603 (2005).

Supplementary Text 2

Methods and Results

Zircon U-Pb geochronology

High-precision zircon U-Pb analyses using chemical abrasion-isotope dilution-isotope ratio mass spectrometry (CA-ID-IRMS) were performed on selected crystals (Fig. S12) at the University of California, Davis. The term IRMS is used here to reflect the combined approach of both thermal ionization mass spectrometry (TIMS) for Pb isotope analyses and multi-collection (MC)-ICP-MS for U isotopic measurements. Detailed methods for CA-ID-IRMS analysis following Mattinson (1) can be found in Zhou, et al. (2, 3), and Lan, et al. (4). Zircon grains were annealed first at 900°C and subsequently analyzed by laser ablation ICP-MS for U-Pb geochronology. These were performed to identify any detrital or inherited components and to select the youngest population of zircons for the subsequent, time-consuming and labor intensive CA-ID-IRMS analysis.

Subsequently, selected grains were leached for 15 h at 190°C, and a ^{202}Pb - ^{205}Pb - ^{233}U - ^{236}U tracer (5) was added to the abraded zircons prior to dissolution. Pb and U were separated from the matrix elements by standard HCl ion exchange chemistry (6) and Pb was loaded onto zone refined Re filaments with a silica gel activator (7). Pb was analyzed on a *Triton Plus* TIMS (thermal ionization mass spectrometer) at UC Davis. Two measurement protocols were used depending on sample size. CY1_3 and CY4_10 were measured on the secondary electron multiplier (SEM) in peak jumping mode. All other samples were measured with ^{204}Pb in the axial secondary electron multiplier while all other isotopes were collected in Faraday cups coupled with $10^{13}\ \Omega$ resistor amplifier boards. The gain calibration for sample ID starting with CY1 and CY3 followed a protocol described by Trinquier (8), see also Zhou et al. (2). For batch CY4, gain calibration was done with a relay matrix board. The SEM yield was calibrated daily and in batch CY4 confirmed with additional measurement of ^{205}Pb in the axial SEM. U isotope dilution measurements were performed on a *Neptune Plus MC-ICP-MS* (Multi-collector inductively-coupled plasma mass spectrometer) at UC Davis using an ESI APEX introduction system. Faraday cups measuring ^{238}U and ^{235}U were coupled with $10^{12}\ \Omega$ resistors and ^{233}U and ^{236}U were coupled with $10^{11}\ \Omega$ resistors. Measurements were corrected for instrumental mass dependent fractionation using an exponential law based on the known ^{233}U - ^{236}U ratio of IRMM-3636 (9). The $^{238}\text{U}/^{236}\text{U}$ ratio of the samples was additionally corrected using the known $^{238}\text{U}/^{235}\text{U}$ ratio of CRM 112a of 137.837 (10) using a linear correction based on sample-standard bracketing. Total procedural blank for U is 0.1 pg. All non-radiogenic

Pb was attributed to laboratory contamination. U-Pb ages and uncertainties were calculated using the algorithms of Schmitz and Schoene (11). We report three levels of uncertainty for the age data, representing analytical uncertainty only (X), analytical and tracer calibration uncertainties (Y), and analytical and tracer and decay constant uncertainties (Z), respectively (12). For U-Pb age comparison within the same laboratory, the first uncertainty is sufficient. To compare U-Pb dates across different laboratories, the second uncertainty should be used. When comparing dates across different methods (e.g., U-Pb vs. Ar-Ar dates), the third uncertainty should be used. Weighted averages and concordia diagrams were produced using Isoplot (13) (Figs. 4 and S13).

The zircons from samples (CY17-9 and CY17-18) show similar features. Rounded and prismatic grains are both present in those samples. The laser ablation ICP-MS analyses confirmed the presence of detrital zircon component. Some analyses are slightly discordant due to common Pb on the surface of unpolished grains, and thus do not provide reliable age information. Concordant dates ranged in age from ~2.5 Ga to 121 Ma, and ~2.2 Ga to ~120 Ma, respectively (Figs. S11a-b). For the sample CY17-9 which was collected from the bottom of the LJT Unit, CA-ID-IRMS of four selected grains (Fig. S12) overlap within error and yield a weighted-mean $^{206}\text{Pb}/^{238}\text{U}$ age of $125.755 \pm 0.061/0.072/0.27$ Ma ($n = 4$, mean square weighted deviation [MSWD] = 1.11) (Fig. S13a-b). Similarly, for the sample CY17-18 which was collected from the top of the LJT Unit, four zircon grains yield a weighted-mean $^{206}\text{Pb}/^{238}\text{U}$ age of $125.684 \pm 0.060/0.072/0.27$ Ma ($n = 4$, MSWD = 1.07) (Fig. S13c-d).

The zircon grains from two tuff samples (CY17-17 and CY18-20) are light yellow and transparent in color, most of the grains are prismatic (Fig. S12). LA-ICP-MS analyses revealed a minor detrital component of zircons ranging in age from ~212 Ma to ~120 Ma, and ~145 Ma to ~120 Ma, respectively (Figs. S11c-d). Selected single zircon grains from the youngest (~120 Ma) group were analyzed by CA-ID-IRMS. The data from sample CY17-17 are in good agreement with each other and yield a weighted-mean $^{206}\text{Pb}/^{238}\text{U}$ age of $125.457 \pm 0.051/0.064/0.27$ Ma ($n = 5$, MSWD = 0.61) (Fig. S13e-f). Five grains from CY18-20 yield a weighted-mean $^{206}\text{Pb}/^{238}\text{U}$ age of $124.122 \pm 0.048/0.062/0.27$ Ma ($n = 5$, MSWD = 0.2) (Fig. S13g-h).

The synthetic standard solution from the EARTHTIME project of 100 Ma, yielded a $^{206}\text{Pb}/^{238}\text{U}$ date of 100.120 ± 0.064 Ma ($n = 4$). Temora zircons yielded a $^{206}\text{Pb}/^{238}\text{U}$ date of 417.01 ± 0.24 Ma ($n = 4$). For the standards, Pb and U were separated in the same way as the samples and measured with the same procedures.

Bulk-rock mineralogical and geochemical analyses

Bulk-rock analyses have been conducted on eight samples collected from LJT, JSG and Huanghuashan units (LJT Unit: CY17-9, CY17-10, and CY17-18; JSG Unit: CY17-16, CY17-17, CY17-23 and CY17-24; Huanghuashan Unit: CY18-20). Sample chips obtained from the central parts of the rocks were handpicked and chosen for further cleaning. The chips were leached with 2% HCl and washed ultrasonically in deionized water before dried and powdered to 200 mesh in a corundum mill.

Mineral assemblages. Determinations of clay mineral assemblages were carried out on un-oriented powder mounts by X-ray diffraction (XRD; Bruker D8 Advance) at the Guangzhou Institute of Geochemistry, Chinese Academy of Sciences. Qualitative and semi-quantitative characterization of mineralogy is based on peak intensity measurements on X-ray patterns, and the diagnostic peak and correction intensity factor were obtained for each mineral. The results are listed in Table S3. The JSG samples (CY17-16, CY17-17, CY17-23 and CY17-24) are mainly composed of clay mineral (smectite; 87.7% – 94.9%), with a small amount of clastic materials. The samples contain minor quartz (0 – 1.3%) and feldspar (3.1% – 11.2%). Besides, CY17-24 contains some calcite (6.1%). In contrast, the LJT samples (CY17-9, CY17-10, and CY17-18) are mainly composed of clay minerals (illite, smectite, and its intermediate product; 25.2% – 62%), with plenty of clastic materials. Each sample contains abundant quartz and feldspar (38% – 63.4%). Additionally, CY17-9 is rich in calcite (34.4%).

Major and trace elemental compositions. Samples were analyzed for major and trace elemental compositions at the Wuhan Sample Solution Analytical Technology Co., Ltd., Wuhan, China. Major element analyses were conducted on X-ray fluorescence spectroscopy (XRF) on fused glass disks using a Rigaku Primus II XRF instrument. A pre-ignition was used to determine the loss on ignition (LOI) prior to major element analyses. Trace element analyses were determined with Agilent 7700e ICP-MS. Samples from JSG and LJT units are characterized by a high loss on ignition (LOI) contents (2.94% – 17.49%; Table S4), consistent with the high percentage of clay minerals. The chemical compositions are characterized by high Al_2O_3 (10.00% – 17.05%), low TiO_2 (0.13% – 0.64%), MnO (0.02% – 0.41%), P_2O_5 (0.05% – 0.17%), and alkalis contents ($\text{Na}_2\text{O} + \text{K}_2\text{O}$; 2.90% – 6.55%). More specifically, the samples (CY17-9 and CY17-24) with the lowest SiO_2 (42.32% and 48.42%) contain the highest CaO (21.45% and 12.21%) and LOI contents (17.49% and 12.92%), which is consistent with high percentage of the calcite. By comparison, the other five samples possess higher SiO_2 (57.92% – 66.98%) and lower CaO contents (2.75% – 3.03%). The Nb/Y-Zr/TiO₂ classification diagram is utilized, since all the selected elements are generally considered to remain immobile during alteration and weathering. All the samples fall within the range of trachyandesite to trachyte (Fig. S14a), suggesting similar original compositions.

The samples have very similar chondrite-normalized (CN; normalization values after Sun and McDonough, (14)) rare earth element (REE) patterns with enrichment of light REE (LREE) over heavy REE (HREE) and pronounced negative Eu anomalies (Fig. S13b). Specifically, samples from JSG Unit display a more fractionated REE pattern $[(La/Yb)_{CN} = 23.91 - 45.76]$ and stronger negative Eu anomalies $[\delta Eu = 0.51 - 0.62; \delta Eu = Eu_{CN}/(Sm_{CN} + Gd_{CN})^{1/2}]$ than that of the samples from LJT Unit $[(La/Yb)_{CN} = 12.80 - 17.88; \delta Eu = 0.67 - 0.80]$ (Figs. S14b and 15a).

Some elements such as Sc, Th, U, Co and Cr are known to be an indicator for source composition (15). For instance the Th/Sc ratio is considered unaffected by sedimentary processes (16) and represents a useful indicator of source rocks. Thus, the diagnostic parameters, i.e., Th/Sc, Zr/Sc, and Co/Ni are selected as proxies for the source characterization. The JSG and LJT samples, as well as the andesites and basalts from the same units (17-19), form a linear correlation in the Zr/Sc-Th/Sc diagram (Fig. S15b). The plot of Th/Sc *versus* Co/Ni distinguishes between JSG and LJT samples, as the former are characterized by higher Th/Sc and lower Co/Ni ratios (Fig. S15c). In addition, the JSG and LJT samples fall into different areas in the Th-Hf-Co ternary diagram, which is commonly used to discriminate the provenance of sedimentary rocks (15) (Fig. S15d).

References

1. J. M. Mattinson, Zircon U–Pb chemical abrasion (“CA-TIMS”) method: Combined annealing and multi-step partial dissolution analysis for improved precision and accuracy of zircon ages. *Chem. Geol.* 220, 47–66 (2005).
2. C. M. Zhou, M. H. Huyskens, X. G. Lang, S. H. Xiao, Q. Z. Yin, Calibrating the terminations of Cryogenian global glaciations. *Geology* 251, 251–254 (2019).
3. C. M. Zhou, M. H. Huyskens, S. H. Xiao, Q. Z. Yin, Refining the termination age of the Cryogenian Sturtian glaciation in South China. *Palaeoworld* 29, 462–468 (2020).
4. Z. W. Lan, M. H. Huyskens, K. Lu, X. H. Li, G. Y. Zhang, D. B. Lu, Q. Z. Yin, Toward refining the onset age of Sturtian glaciation in South China. *Precambrian Res.* 338, 105555 (2020).
5. M. H. Huyskens, S. Zink, Y. Amelin, Evaluation of temperature-time conditions for the chemical abrasion treatment of single zircons for U–Pb geochronology. *Chem. Geol.* 438, 25–35 (2016).
6. T. Krogh, A low-contamination method for hydrothermal decomposition of zircon and extraction of U and Pb for isotopic age determinations. *Geochim. Cosmochim. Ac.* 37, 485–494 (1973).
7. M. H. Huyskens, T. Iizuka, Y. Amelin, Evaluation of colloidal silicagels for lead isotopic measurements using thermal ionisation mass spectrometry. *J. Anal. Atom. Spectrom.* 27, 1439–1446 (2012).
8. A. Trinquier, Fractionation of Oxygen Isotopes by Thermal Ionization Mass Spectrometry Inferred from Simultaneous Measurement of $^{17}\text{O}/^{16}\text{O}$ and $^{18}\text{O}/^{16}\text{O}$ Ratios and Implications for the ^{182}Hf - ^{182}W Systematics: *Anal. Chem.* 88, 5600–5604 (2016).
9. A. Verbruggen, A. Alonso, R. Eykens, F. Kehoe, H. Kühn, S. Richter, Y. Aregbe, Preparation and Certification of IRMM 3636, IRMM 3636a and IRMM 3636b. OPOCE, 24pp (2008).
10. S. Richter, R. Eykens, H. Kühn, Y. Aregbe, A. Verbruggen, S. Weyer, New average values for the $n(^{238}\text{U})/n(^{235}\text{U})$ isotope ratios of natural uranium standards: *Int. J. Mass Spectrom.* 295, 94–97 (2010).
11. M. D. Schmitz, B. Schoene, Derivation of isotope ratios, errors, and error correlations for U–Pb geochronology using ^{205}Pb - ^{235}U - ^{233}U spiked isotope dilution thermal ionization mass spectrometric data. *Geochem. Geophys. Geosy.* 8, Q08006 (2007).
12. I. M. Villa, M. L. Bonardi, P. De Bièvre, N. E. Holden, P. R. Renne, IUPAC-IUGS status report on the half-lives of ^{238}U , ^{235}U and ^{234}U : *Geochim. Cosmochim. Ac.* 172, 387–392 (2016).
13. K. Ludwig, Isoplot 3.75. A Geochronological toolkit for Microsoft Excel. Berkeley Geochronology Center, *Spec. Pub.* 5 (2012).
14. S. S. Sun, W. F. McDonough, Chemical and Isotopic Systematics of Oceanic Basalts: Implications for Mantle Composition and Processes. *Geol. Soc. Spec. Pub.* 42, 313–345 (1989).
15. S. R. Taylor, S. M. McLennan, The continental crust: its composition and evolution. Black Scientific Publications, pp. 1–312 (1985).
16. S. M. McLennan, S. Hemming, D. K. McDaniel, G. N. Hanson, Geochemical approaches to sedimentation, provenance, and tectonics, in Johnson, M.J., and Basu, A., eds., Processes Controlling the Composition of Clastic Sediments. *Geol. Soc. Spec. Paper* 284, 21–40 (1993).
17. X. R. Wang, S. Gao, X. M. Liu, H. L. Yuan, Z. C. Hu, H. Zhang, X. C. Wang, Geochemistry of high-Mg andesites from the early Cretaceous Yixian Formation, western Liaoning: Implications for lower crustal delamination and Sr/Y variations. *Sci. China D* 49, 904–914 (2006).
18. S. Gao, R. L. Rudnick, W. L. Xu, H. L. Yuan, Y. S. Liu, R. J. Walker, I. S. Puchtel, X. M. Liu, H. Huang, X. R. Wang, J. Yang, Recycling deep cratonic lithosphere and generation of intraplate magmatism in the North China Craton. *Earth Planet. Sc. Lett.* 270, 41–53 (2008).

19. W. Yang, S. G. Li, Geochronology and geochemistry of the Mesozoic volcanic rocks in Western Liaoning: Implications for lithospheric thinning of the North China Craton. *Lithos* 102, 88-117 (2008).

Supplementary Text 3

Cyclicality of the Jianshangou lacustrine deposits

The refined duration of the Yixian Formation also yields important insights on the duration of the JSG lacustrine deposits. The sedimentary cyclicality was interpreted as periodic lake-level fluctuations plausibly caused by climatic changes that in turn may be orbitally forced Milankovitch cycles (1,2). Both studies (1,2) observed ~2 m cycle, and ~1 m cycle, and Wu et al. (2) observed additional 50-67 cm and 18-42 cm higher frequency cycles based on anhysteretic remanent magnetization and magnetic susceptibility at the Sihetun section. Wang et al. (1) hypothesized that their ~2 m cycles reflect obliquity forcing (~37 kyr), and their ~1 m cycles reflect the climatic precession cycle (~20 kyr), whereas Wu et al. (2) argued that the ~2 m cycles reflect the ~100 kyr cycles (1.7 cm/kyr sedimentation rate) of short eccentricity (c.f. Fig. 3 in ref. 2). The two different interpretation would have huge impact on the actual duration estimates of the JSG Unit, with Wang et al. (1) suggesting a total duration of ~820 or ~410 Kyr for the 41 m JSG unit from their drill core study (see Fig. 3 in Wang et al. (1), and discussion related to their Fig. 22), whereas the accumulation rate derived from Wu et al. (2) predicts a duration of the same stratigraphic interval of >2 Myr. Our new data indicate that the entire Yixian Formation is only 1.633 ± 0.078 Myr max, which means that the JSG Unit within Yixian Formation should be <1.633 Myr. This would clearly exclude the possibility to interpret the 2 m cycle as 100 Kyr eccentricity cycle. It is entirely possible that the sedimentation rates of lacustrine environments between the studied outcrops and drill cores (1,2, and this study) are highly variable, obtaining accurate Milankovitch cycle signals from the terrestrial sediments remain a challenging goal without further high resolution and high precision geochronological constraints.

References

1. Y. Q. Wang, P. E. Olsen, J. G. Sha, X. G. Yao, H. Y. Liao, Y. H. Pan, S. Kinney, X. L. Zhang, X. Rao, Stratigraphy, correlation, depositional environments, and cyclicity of the Early Cretaceous Yixian and ?Jurassic-Cretaceous Tuchengzi formations in the Sihetun area (NE China) based on three continuous cores. *Palaeogeogr Palaeoclimatol Palaeoecol* 464, 110–133 (2016).
2. H. C. Wu, S. H. Zhang, G. Q. Jiang, T. S. Yang, J. H., Guo, H. Y. Li. Astrochronology for the Early Cretaceous Jehol Biota in northeastern China. *Palaeogeogr Palaeoclimatol Palaeoecol* 385, 221–228 (2013).

Table S1. Summary of literature age dates from the Yixian Formation in western Liaoning.

| Unit / Sample name | Lithology | Method | Mineral | Age (Ma \pm 2 σ) | Recalculated age* (Ma \pm 2 σ) [inc. decay constants] | References |
|----------------------------|------------------|------------------------------------|-------------|-------------------------------|-----------------------------------------------------------------------|------------|
| Jiufotang Formation | | | | | | |
| L3001 | tuff | SHRIMP U-Pb | zircon | 124 \pm 4 | 124 \pm 4 | (1) |
| Lx9 | tuff | ⁴⁰ Ar/ ³⁹ Ar | K-feldspar | 120.1 \pm 0.4 | 121.2 \pm 0.7 | (1) |
| JFT07-1 | tuff | ⁴⁰ Ar/ ³⁹ Ar | sanidine | 122.1 \pm 0.3 | 123.4 \pm 0.6 | (2) |
| Yixian Formation | | | | | | |
| Huanghuashan Unit | | | | | | |
| YX291 | rhyolite | LA-ICP-MS | zircon | 119.8 \pm 3.8 | 119.8 \pm 3.8 | (3) |
| YX275 | rhyolite | LA-ICP-MS | zircon | 118.9 \pm 2.8 | 118.9 \pm 2.8 | (3) |
| 6 | volcanic breccia | ⁴⁰ Ar/ ³⁹ Ar | plagioclase | 121.5 \pm 1.8 | 121.7 \pm 2.1 | (4) |
| 6 | volcanic breccia | ⁴⁰ Ar/ ³⁹ Ar | biotite | 121.6 \pm 1.0 | 121.8 \pm 1.3 | (4) |
| Upper Lava Unit | | | | | | |
| ZCZ28 | andesite | ⁴⁰ Ar/ ³⁹ Ar | groundmass | 122.0 \pm 1.3 | 122.9 \pm 1.1 | (5) |
| Mt14 | andesite | ⁴⁰ Ar/ ³⁹ Ar | groundmass | 120.2 \pm 1.5 | 120.2 \pm 1.5 | (5) |
| Mt9 | andesite | ⁴⁰ Ar/ ³⁹ Ar | groundmass | 121.2 \pm 1.3 | 121.2 \pm 1.3 | (5) |
| | basalt | ⁴⁰ Ar/ ³⁹ Ar | groundmass | 123.7 \pm 0.9 | 123.7 \pm 0.9 | (6) |
| Jianshangou Unit | | | | | | |
| YX07-3 | tuff | ⁴⁰ Ar/ ³⁹ Ar | sanidine | 122.9 \pm 0.7 | 124 \pm 0.9 | (2) |
| 99L-HDZ1 | tuff | ⁴⁰ Ar/ ³⁹ Ar | sanidine | 125.0 \pm 0.38 | 126.2 \pm 0.8 | (7) |

| Unit / Sample name | Lithology | Method | Mineral | Age (Ma \pm 2 σ) | Recalculated age* (Ma \pm 2 σ) [inc. decay constants] | References |
|------------------------|-------------------|---------------------------------|------------|-------------------------------|-----------------------------------------------------------------------|------------|
| LX-HBJ-6 | tuff | SHRIMP U-Pb | zircon | 122.8 \pm 1.6 | 122.8 \pm 1.6 | (8) |
| YX07-4 | tuff | $^{40}\text{Ar}/^{39}\text{Ar}$ | sanidine | 124.1 \pm 0.4 | 125.3 \pm 0.7 | (2) |
| P1T-2 | tuff | TIMS U-Pb | zircon | 125.65 \pm 0.17 | 125.65 \pm 0.31 | (9) |
| P1T-2 | tuff | $^{40}\text{Ar}/^{39}\text{Ar}$ | sanidine | 124.6 \pm 0.6 | 125.8 \pm 0.7 | (10) |
| P4T-1 | tuff | $^{40}\text{Ar}/^{39}\text{Ar}$ | sanidine | 124.6 \pm 0.4 | 125.8 \pm 0.8 | (10) |
| LX-SHT-12 | tuff | SHRIMP U-Pb | zircon | 124.7 \pm 2.7 | 124.7 \pm 2.7 | (8) |
| 99L-S1 | tuff | $^{40}\text{Ar}/^{39}\text{Ar}$ | sanidine | 125.0 \pm 0.36 | 126.2 \pm 0.8 | (7) |
| YL31 | tuff | TIMS U-Pb | zircon | 125.2 \pm 0.9 | 125.2 \pm 0.9 | (11) |
| Lower Lava Unit | | | | | | |
| | basalt | $^{40}\text{Ar}/^{39}\text{Ar}$ | groundmass | 125.0 \pm 1.4 | 125 \pm 1.4 | (6) |
| YX07-2 | basalt | $^{40}\text{Ar}/^{39}\text{Ar}$ | groundmass | 126.2 \pm 0.4 | 127.3 \pm 0.8 | (2) |
| YX07-6 | basalt | $^{40}\text{Ar}/^{39}\text{Ar}$ | groundmass | 129.7 \pm 0.5 | 130.9 \pm 0.8 | (2) |
| YL29 | basaltic andesite | $^{40}\text{Ar}/^{39}\text{Ar}$ | whole rock | 128.2 \pm 1.6 | 131.3 \pm 1.8 | (12) |
| SYNU-005 | basalt | $^{40}\text{Ar}/^{39}\text{Ar}$ | groundmass | 126.0 \pm 0.8 | 126 \pm 1.1 | (13) |
| SYNU-010 | basalt | $^{40}\text{Ar}/^{39}\text{Ar}$ | groundmass | 125.8 \pm 1.0 | 125.8 \pm 1 | (13) |
| Lujiatun Unit | | | | | | |
| L3004 | tuff | $^{40}\text{Ar}/^{39}\text{Ar}$ | K-feldspar | 123.3 \pm 1.3 | 124.2 \pm 1.8 | (14) |
| L3003 | tuff | $^{40}\text{Ar}/^{39}\text{Ar}$ | K-feldspar | 123.0 \pm 1.4 | 124.5 \pm 1.9 | (14) |
| LX-HBJ-1 | tuff | SHRIMP U-Pb | zircon | 124.9 \pm 1.7 | 124.9 \pm 1.7 | (8) |

* Recalculated age is after Olierook et al (15).

Table S2. U-Pb isotopic data of analyzed single zircon grains by CA-ID-IRMS.

| Sample / Analysis ID | Compositional Parameters | | | | Radiogenic Isotope Ratios | | | | | | | | Isotopic Ages | | | | | |
|----------------------------|--------------------------|-------------------------|-------------------------|-----------------------------------------|-----------------------------------------|-----------------------------------------|----------|----------------------------------------|----------|----------------------------------------|----------|----------------------------|-----------------------------------------|-----|----------------------------------------|------|----------------------------------------|------|
| | Th/ U | Pb*/ Pb _c | Pb _c (pg) | ²⁰⁶ Pb/ ²⁰⁴ Pb | ²⁰⁸ Pb/ ²⁰⁶ Pb | ²⁰⁷ Pb/ ²⁰⁶ Pb | % err | ²⁰⁷ Pb/ ²³⁵ U | % err | ²⁰⁶ Pb/ ²³⁸ U | % err | correlation coefficient | ²⁰⁷ Pb/ ²⁰⁶ Pb | ± | ²⁰⁷ Pb/ ²³⁵ U | ± | ²⁰⁶ Pb/ ²³⁸ U | ± |
| | (a) | (b) | (b) | (c) | (d) | (d) | (e) | (d) | (e) | (d) | (e) | | (f) | (e) | (f) | (e) | (f) | (e) |
| CY17-9 | | | | | | | | | | | | | | | | | | |
| CY1_6 | 0.47 | 11.99 | 1.0 | 765.8 | 0.1485 | 0.0484 | 0.87 | 0.1314 | 0.93 | 0.0197 | 0.08 | 0.78 | 116 | 21 | 125.31 | 1.10 | 125.80 | 0.10 |
| CY1_7 | 0.46 | 12.66 | 0.9 | 808.2 | 0.1472 | 0.0486 | 0.91 | 0.1319 | 0.97 | 0.0197 | 0.10 | 0.70 | 127 | 21 | 125.77 | 1.15 | 125.71 | 0.12 |
| CY1_8 | 0.73 | 16.47 | 0.9 | 977.5 | 0.2322 | 0.0487 | 1.11 | 0.1322 | 1.19 | 0.0197 | 0.09 | 0.83 | 132 | 26 | 126.06 | 1.41 | 125.77 | 0.11 |
| CY1_9 | 0.70 | 2.57 | 4.0 | 168.7 | 0.2231 | 0.0484 | 2.94 | 0.1312 | 3.11 | 0.0197 | 0.23 | 0.78 | 118 | 69 | 125.17 | 3.66 | 125.56 | 0.28 |
| CY17-18 | | | | | | | | | | | | | | | | | | |
| CY1_1 | 0.79 | 17.55 | 1.6 | 1018.1 | 0.2538 | 0.0489 | 0.52 | 0.1327 | 0.56 | 0.0197 | 0.06 | 0.66 | 141 | 12 | 126.49 | 0.67 | 125.71 | 0.08 |
| CY1_2 | 0.63 | 7.53 | 1.1 | 464.8 | 0.2041 | 0.0492 | 1.41 | 0.1334 | 1.51 | 0.0197 | 0.10 | 0.99 | 156 | 33 | 127.13 | 1.80 | 125.59 | 0.13 |
| CY1_3 | 1.01 | 4.06 | 1.5 | 238.1 | 0.3227 | 0.0487 | 3.86 | 0.1323 | 4.10 | 0.0197 | 0.29 | 0.85 | 134 | 91 | 126.16 | 4.87 | 125.75 | 0.36 |
| CY4_10 | 0.60 | 4.88 | 2.7 | 311.6 | 0.1889 | 0.0481 | 1.68 | 0.1306 | 1.81 | 0.0197 | 0.17 | 0.80 | 105 | 40 | 124.66 | 2.12 | 125.70 | 0.21 |
| CY17-17 | | | | | | | | | | | | | | | | | | |
| CY3_6 | 1.04 | 10.36 | 1.4 | 579.0 | 0.3298 | 0.0482 | 0.98 | 0.1307 | 1.05 | 0.0197 | 0.09 | 0.77 | 110 | 23 | 124.69 | 1.23 | 125.45 | 0.11 |
| CY3_7 | 1.08 | 4.92 | 3.5 | 282.8 | 0.3409 | 0.0482 | 2.43 | 0.1306 | 2.57 | 0.0197 | 0.16 | 0.89 | 108 | 57 | 124.64 | 3.02 | 125.53 | 0.20 |
| CY3_8 | 1.12 | 9.30 | 1.4 | 512.9 | 0.3531 | 0.0481 | 1.15 | 0.1304 | 1.22 | 0.0197 | 0.09 | 0.83 | 104 | 27 | 124.44 | 1.43 | 125.51 | 0.11 |
| CY3_9 | 1.05 | 10.68 | 1.3 | 593.2 | 0.3356 | 0.0488 | 1.06 | 0.1322 | 1.13 | 0.0197 | 0.08 | 0.85 | 138 | 25 | 126.08 | 1.34 | 125.45 | 0.10 |
| CY3_10 | 1.48 | 10.70 | 1.1 | 542.7 | 0.4725 | 0.0486 | 1.20 | 0.1316 | 1.28 | 0.0196 | 0.09 | 0.94 | 128 | 28 | 125.52 | 1.51 | 125.40 | 0.11 |
| CY18-20 | | | | | | | | | | | | | | | | | | |
| CY4_2 | 1.2 | 57.9 | 0.9 | 3037.5 | 0.3726 | 0.0485 | 0.26 | 0.1299 | 0.28 | 0.0194 | 0.05 | 0.53 | 122 | 6 | 124.03 | 0.33 | 124.11 | 0.06 |
| CY4_6 | 1.1 | 10.1 | 4.0 | 554.1 | 0.3501 | 0.0485 | 1.02 | 0.1299 | 1.10 | 0.0194 | 0.09 | 0.85 | 121 | 24 | 124.00 | 1.28 | 124.16 | 0.11 |
| CY4_7 | 1.1 | 3.6 | 2.5 | 208.6 | 0.3596 | 0.0477 | 2.64 | 0.1278 | 2.84 | 0.0194 | 0.23 | 0.89 | 82 | 63 | 122.08 | 3.27 | 124.15 | 0.28 |
| CY4_8 | 1.0 | 6.8 | 2.3 | 391.3 | 0.3141 | 0.0485 | 1.38 | 0.1300 | 1.49 | 0.0194 | 0.13 | 0.85 | 124 | 32 | 124.08 | 1.74 | 124.10 | 0.16 |
| CY4_9 | 1.0 | 7.1 | 3.2 | 400.9 | 0.3304 | 0.0486 | 1.68 | 0.1301 | 1.79 | 0.0194 | 0.18 | 0.69 | 126 | 39 | 124.23 | 2.10 | 124.13 | 0.22 |

(a) Model Th/U ratio calculated from radiogenic ²⁰⁸Pb/²⁰⁶Pb ratio and ²⁰⁷Pb/²³⁵U age;

(b) Pb* and Pb_c represent radiogenic and common Pb, respectively;

(c) Measured ratio corrected for spike and fractionation only;

(d) Corrected for fractionation, spike, and common Pb; all common Pb was assumed to be blank with a composition of ²⁰⁶Pb/²⁰⁴Pb = 16.96 ± 0.35; ²⁰⁷Pb/²⁰⁴Pb = 14.48 ± 0.29; ²⁰⁸Pb/²⁰⁴Pb = 35.03 ± 0.7;

(e) Errors are 2-sigma, propagated using the algorithms of Schmitz and Schoene (16) and Crowley et al. (17);

(f) Calculations are based on the decay constants of Jaffey et al. (18) and a ²³⁸U/²³⁵U ratio of 137.818 (Hiess et al. (19)).

Table S3. Mineral compositions (%) of the volcanic tuff samples from Lujiatun and Jianshangou units.

| Sample | Illite | Smectite | I-S* | Quartz | Feldspar | Calcite | Zeolite |
|-------------------------|--------|----------|------|--------|----------|---------|---------|
| Lujiatun Unit | | | | | | | |
| CY17-9 | 4.4 | | 20.8 | 8.8 | 31.6 | 34.4 | |
| CY17-10 | 8.2 | | 26.7 | 25.6 | 37.8 | | 1.6 |
| CY17-18 | | 62 | | 11.1 | 26.9 | | |
| Jianshangou Unit | | | | | | | |
| CY17-16 | | 94.9 | | 0.8 | 4.3 | | |
| CY17-17 | | 91.5 | | 1.3 | 7.2 | | |
| CY17-23 | | 87.7 | | 1 | 11.2 | | |
| CY17-24 | | 90.8 | | | 3.1 | 6.1 | |

I-S*: Intermediate product between illite and smectite

Table S4. Major and trace elements compositions (%) of the volcanic tuff samples from Lujiatun, Jianshangou and Huanghuashan units.

| Sample | CY17-9 | CY17-10 | CY17-18 | CY17-16 | CY17-23 | CY17-24 | CY17-17 | CY18-20 |
|--------------------------------|----------------------|---------|---------|-------------------------|---------|---------|--------------------------|---------|
| | Lujiatun Unit | | | Jianshangou Unit | | | Huanghuashan Unit | |
| Major elements | | | | | | | | |
| SiO ₂ | 42.32 | 66.98 | 63.88 | 57.92 | 60.37 | 48.42 | 60.09 | 64.53 |
| TiO ₂ | 0.17 | 0.50 | 0.64 | 0.24 | 0.23 | 0.13 | 0.23 | 0.50 |
| Al ₂ O ₃ | 10.00 | 14.59 | 15.16 | 16.35 | 16.06 | 13.38 | 17.05 | 18.27 |
| Fe ₂ O ₃ | 1.68 | 3.42 | 4.22 | 7.61 | 3.71 | 5.48 | 4.37 | 2.75 |
| MnO | 0.41 | 0.05 | 0.03 | 0.05 | 0.02 | 0.13 | 0.04 | 0.03 |
| MgO | 1.05 | 1.70 | 3.79 | 5.05 | 5.56 | 4.18 | 4.40 | 0.60 |
| CaO | 21.45 | 2.76 | 2.75 | 2.81 | 2.88 | 12.21 | 3.03 | 1.74 |
| Na ₂ O | 1.93 | 2.95 | 2.03 | 1.11 | 1.15 | 1.08 | 1.92 | 6.31 |
| K ₂ O | 2.80 | 3.61 | 2.11 | 1.94 | 2.09 | 1.82 | 2.47 | 4.19 |
| P ₂ O ₅ | 0.11 | 0.17 | 0.17 | 0.08 | 0.05 | 0.05 | 0.05 | 0.18 |
| L.O.I | 17.49 | 2.94 | 4.91 | 7.10 | 7.41 | 12.92 | 6.40 | 0.70 |
| Total | 99.43 | 99.67 | 99.67 | 100.25 | 99.52 | 99.79 | 100.04 | 99.81 |
| Trace elements | | | | | | | | |
| Li | 24.5 | 34.9 | 60.4 | 124 | 117 | 76.5 | 95.0 | 12.4 |
| Be | 1.55 | 2.24 | 2.27 | 1.70 | 2.05 | 1.49 | 1.89 | 2.23 |
| Sc | 3.16 | 6.86 | 9.07 | 4.95 | 4.77 | 3.49 | 3.88 | 4.94 |
| V | 19.9 | 48.0 | 68.5 | 19.2 | 18.0 | 16.7 | 18.2 | 40.9 |
| Cr | 12.3 | 30.7 | 54.5 | 37.6 | 5.28 | 1.88 | 0.81 | 85.0 |
| Co | 4.74 | 6.80 | 15.3 | 5.47 | 4.48 | 8.45 | 4.01 | 5.61 |
| Ni | 11.3 | 13.6 | 28.0 | 41.5 | 15.3 | 35.1 | 14.8 | 15.3 |
| Cu | 5.32 | 10.4 | 16.5 | 13.1 | 3.81 | 6.30 | 4.13 | 11.7 |
| Zn | 27.0 | 57.4 | 61.7 | 92.8 | 45.4 | 52.1 | 46.9 | 46.9 |
| Ga | 13.1 | 18.7 | 19.5 | 21.2 | 21.5 | 14.7 | 21.6 | 17.2 |
| Rb | 76.3 | 125 | 88.2 | 47.2 | 53.4 | 33.7 | 45.9 | 137 |
| Sr | 291 | 445 | 541 | 283 | 185 | 157 | 293 | 478 |
| Y | 12.5 | 23.1 | 18.3 | 8.46 | 8.07 | 11.4 | 14.6 | 9.94 |

| Sample | CY17-9 | CY17-10 | CY17-18 | CY17-16 | CY17-23 | CY17-24 | CY17-17 | CY18-20 |
|-----------------------|---------------|---------|---------|------------------|---------|---------|-------------------|---------|
| | Lujiatun Unit | | | Jianshangou Unit | | | Huanghuashan Unit | |
| Zr | 112 | 233 | 179 | 157 | 225 | 127 | 224 | 192 |
| Nb | 12.2 | 14.2 | 12.5 | 13.4 | 16.2 | 9.42 | 13.2 | 14.7 |
| Sn | 1.14 | 1.93 | 1.64 | 2.45 | 2.70 | 2.02 | 2.67 | 36.0 |
| Cs | 1.78 | 5.36 | 3.87 | 0.85 | 1.23 | 1.40 | 0.77 | 0.86 |
| Ba | 383 | 629 | 581 | 682 | 371 | 225 | 804 | 1284 |
| La | 27.4 | 38.3 | 37.0 | 56.4 | 30.3 | 34.0 | 56.5 | 41.9 |
| Ce | 46.1 | 77.3 | 70.2 | 108 | 61.0 | 64.3 | 112 | 76.9 |
| Pr | 5.07 | 8.77 | 8.00 | 10.7 | 6.43 | 6.29 | 11.9 | 7.81 |
| Nd | 17.8 | 32.2 | 28.6 | 34.1 | 22.3 | 21.1 | 41.9 | 26.2 |
| Sm | 3.21 | 6.05 | 5.09 | 5.07 | 3.84 | 3.34 | 7.12 | 4.04 |
| Eu | 0.66 | 1.22 | 1.23 | 0.87 | 0.65 | 0.50 | 1.22 | 0.94 |
| Gd | 2.58 | 4.76 | 4.04 | 3.17 | 2.57 | 2.48 | 4.74 | 2.48 |
| Tb | 0.39 | 0.70 | 0.59 | 0.43 | 0.36 | 0.37 | 0.67 | 0.35 |
| Dy | 2.17 | 4.07 | 3.23 | 2.09 | 1.90 | 2.18 | 3.39 | 1.88 |
| Ho | 0.41 | 0.80 | 0.62 | 0.36 | 0.33 | 0.40 | 0.61 | 0.37 |
| Er | 1.20 | 2.31 | 1.77 | 1.05 | 0.92 | 1.16 | 1.56 | 1.01 |
| Tm | 0.16 | 0.33 | 0.24 | 0.13 | 0.12 | 0.16 | 0.21 | 0.15 |
| Yb | 1.10 | 2.15 | 1.63 | 0.88 | 0.77 | 1.02 | 1.24 | 0.94 |
| Lu | 0.16 | 0.32 | 0.23 | 0.13 | 0.11 | 0.16 | 0.16 | 0.14 |
| Hf | 2.78 | 6.07 | 4.71 | 4.61 | 6.20 | 3.95 | 6.16 | 4.72 |
| Ta | 0.91 | 1.04 | 0.89 | 1.12 | 1.25 | 0.94 | 1.24 | 0.93 |
| Tl | 0.48 | 0.69 | 0.87 | 0.45 | 0.61 | 1.16 | 0.85 | 0.57 |
| Pb | 18.6 | 22.3 | 18.7 | 46.7 | 26.5 | 41.8 | 38.8 | 20.9 |
| Th | 6.34 | 10.5 | 9.16 | 17.1 | 16.0 | 15.2 | 16.0 | 9.39 |
| U | 1.54 | 2.19 | 4.26 | 4.31 | 2.41 | 2.87 | 3.71 | 1.49 |
| ∑REE | 108.51 | 179.32 | 162.48 | 222.99 | 131.58 | 137.46 | 243.69 | 165.11 |
| δEu | 0.68 | 0.67 | 0.80 | 0.62 | 0.59 | 0.51 | 0.61 | 0.84 |
| (La/Yb) _{CN} | 17.88 | 12.80 | 16.31 | 45.76 | 28.21 | 23.91 | 32.56 | 31.98 |

References

1. H. Y. He, X. L. Wang, Z. H. Zhou, F. Wang, A. Boven, G. H. Shi, R. X. Zhu, Timing of the Jiufotang Formation (Jehol Group) in Liaoning, northeastern China, and its implications. *Geophys. Res. Lett.* 31, L12605 (2004).
2. S. C. Chang, H. Zhang, P. R. Renne, Y. Fang, High-precision $^{40}\text{Ar}/^{39}\text{Ar}$ age for the Jehol Biota. *Palaeogeogr. Palaeoclimatol. Palaeoecol.* 280, 94–104 (2009).
3. H. Zhang, X. M. Liu, W. Chen, Z. T. Li, F. L. Yang, The age of the top of the Yixian Formation in the Beipiao-Yixian area, western Liaoning, and its importance (in Chinese with English abstract). *Geol. China* 32, 596–603 (2005).
4. P. E. Smith, N. M. Evensen, D. York, M. M. Chang, F. Jin, J. L. Li, S. Cumbaa, D. Russell, Dates and rates in ancient lakes: ^{40}Ar - ^{39}Ar evidence for an Early Cretaceous age for the Jehol Group, northeast China. *Can. J. Earth Sci.* 32, 1426–1431 (1995).
5. H. Y. He, Y. X. Pan, L. Tauxe, H. F. Qin, R. X. Zhu, Toward age determination of the M0r (Barremian-Aptian boundary) of the Early Cretaceous. *Phys. Earth Planet. Interi.* 169, 41–48 (2008).
6. R. X. Zhu, Y. X. Pan, R. Shi, Q. Liu, D. Li, Palaeomagnetic and $^{40}\text{Ar}/^{39}\text{Ar}$ dating constraints on the age of the Jehol Biota and the duration of deposition of the Sihetun fossil-bearing lake sediments, northeast China. *Cret. Res.* 28, 171–176 (2007).
7. C. C. Swisher, X. Wang, Z. H. Zhou, Y. Wang, F. Jin, J. Zhang, X. Xu, F. Zhang, Y. Wang, Further support for a Cretaceous age for the feathered-dinosaur beds of Liaoning, China: New $^{40}\text{Ar}/^{39}\text{Ar}$ dating of the Yixian and Tuchengzi Formations. *Chinese Sci. Bull.* 47, 136–139 (2002).
8. W. Yang, S. G. Li, B. Y. Jiang, New evidence for Cretaceous age of the feathered dinosaurs of Liaoning: zircon U-Pb SHRIMP dating of the Yixian Formation in Sihetun, Northeast China. *Cret. Res.* 28, 177–182 (2007).
9. P. R. Renne, R. Mundil, G. Balco, K. Min, K. R. Ludwig, Joint determination of ^{40}K decay constants and $^{40}\text{K}^*/^{40}\text{K}$ for the Fish Canyon sanidine standard, and improved accuracy for $^{40}\text{K}/^{39}\text{K}$ geochronology. *Geochim. Cosmochim. Ac.* 74, 5349–5367 (2010).
10. C. C. Swisher, Y. Q. Wang, X. L. Wang, X. Xu, Y. Wang, Cretaceous age for the feathered dinosaurs of Liaoning, China. *Nature* 400, 58–61 (1999).
11. S. S. Wang, Y. Q. Wang, H. G. Hu, H. M. Li, The existing time of Sihetun vertebrate in western Liaoning. *Chinese Sci. Bull.* 46, 779–782 (2001).
12. S. S. Wang, H. G. Hu, P. X. Li, Y. Q. Wang, Further discussion on the geologic age of Sihetun vertebrate assemblage in western Liaoning, China: evidence from Ar-Ar dating (in Chinese with English abstract). *Acta Petrol. Sin.* 4, 663–668 (2001).

13. S. C. Chang, K. Q. Gao, C. F. Zhou, F. Jourdan, New chronostratigraphic constraints on the Yixian Formation with implications for the Jehol Biota. *Palaeogeogr. Palaeoclimatol. Palaeoecol.* 487, 399–406 (2017).
14. H. Y. He, X. L. Wang, Z. H. Zhou, F. Jin, F. Wang, L. K. Yang, X. Ding, A. Boven, R. X. Zhu, $^{40}\text{Ar}/^{39}\text{Ar}$ dating of Lujiatun Bed (Jehol Group) in Liaoning, northeastern China. *Geophys. Res. Lett.* 33, L04303 (2006).
15. H. K. Olierook, F. Jourdan, R. Merle, Age of the Barremian–Aptian boundary and onset of the Cretaceous Normal Superchron. *Earth-Sci. Rev.* 197 (2019).
16. M. D. Schmitz, B. Schoene, Derivation of isotope ratios, errors, and error correlations for U-Pb geochronology using ^{205}Pb - ^{235}U -(^{233}U)-spiked isotope dilution thermal ionization mass spectrometric data. *Geochem. Geophys. Geosy.* 8, Q08006 (2007).
17. J. L. Crowley, B. Schoene, S. A. Bowring, U-Pb dating of zircon in the Bishop tuff at the millennial scale. *Geology* 35, 1123–1126 (2007).
18. H. Jaffey, K. F. Flynn, L. Glendeni, W. C. Bentley, A. M. Essling, Precision Measurement of Half-Lives and Specific Activities of ^{235}U and ^{238}U . *Phys. Rev. C* 4, 1889–1906 (1971).
19. J. Hiess, D. J. Condon, N. McLean, S. R. Noble, $^{238}\text{U}/^{235}\text{U}$ Systematics in Terrestrial Uranium-Bearing Minerals. *Science* 335, 1610–1614 (2012).